Mg^{2+} Enhances Voltage Sensor/Gate Coupling in BK Channels

Frank T. Horrigan and Zhongming Ma

Department of Physiology, University of Pennsylvania School of Medicine Philadelphia, PA 19104

BK (Slo1) potassium channels are activated by millimolar intracellular Mg^{2+} as well as micromolar Ca^{2+} and membrane depolarization. Mg^{2+} and Ca^{2+} act in an approximately additive manner at different binding sites to shift the conductance–voltage (G_K-V) relation, suggesting that these ligands might work through functionally similar but independent mechanisms. However, we find that the mechanism of Mg^{2+} action is highly dependent on voltage sensor activation and therefore differs fundamentally from that of Ca^{2+}. Evidence that Ca^{2+} acts independently of voltage sensor activation includes an ability to increase open probability (P_O) at extreme negative voltages where voltage sensors are in the resting state; 2 μM Ca^{2+} increases P_O more than 15-fold at −120 mV. However 10 mM Mg^{2+}, which has an effect on the G_K-V relation similar to 2 μM Ca^{2+}, has no detectable effect on P_O when voltage sensors are in the resting state. Gating currents are only slightly altered by Mg^{2+} when channels are closed, indicating that Mg^{2+} does not act merely to promote voltage sensor activation. Indeed, channel opening is facilitated in a voltage-independent manner by Mg^{2+} in a mutant (R210C) whose voltage sensors are constitutively activated. Thus, 10 mM Mg^{2+} increases P_O only when voltage sensors are activated, effectively strengthening the allosteric coupling of voltage sensor activation to channel opening. Increasing Mg^{2+} from 10 to 100 mM, to occupy very low affinity binding sites, has additional effects on gating that more closely resemble those of Ca^{2+}. The effects of Mg^{2+} on steady-state activation and I_K kinetics are discussed in terms of an allosteric gating scheme and the state-dependent interactions between Mg^{2+} and voltage sensor that may underlie this mechanism.

INTRODUCTION

The activity of BK-type Ca^{2+}-activated K^+ channels is important for the function of nerve, muscle, and secretory cells (Vergara et al., 1998). BK channels respond to two primary signals, membrane voltage and intracellular Ca^{2+}, but are also sensitive to a variety of regulatory ligands, including intracellular Mg^{2+} (Shi and Cui, 2001; Zhang et al., 2001), heme (Tang et al., 2003), and protons (Avdonin et al., 2003), that can influence channel gating under physiological and/or pathophysiological conditions. Therefore, to understand how BK channel activity is regulated it is important to understand how these signaling and regulatory factors affect channel gating and interact with each other. Previous studies suggest that millimolar $[Mg^{2+}]_i$ and micromolar $[Ca^{2+}]_i$ activate BK channels through similar functional mechanisms (Shi and Cui, 2001; Zhang et al., 2001). Here we show that the action of Mg^{2+} differs from that of Ca^{2+} in its dependence on voltage sensor activation. The results highlight that multiple pathways of communication exist between the transmembrane and cytosolic domains of BK channels.

That Ca^{2+} and voltage act independently to regulate opening is evident from BK channel function and consistent with channel structure. BK channels can be fully activated by membrane depolarization in the absence of Ca^{2+} (Cui et al., 1997), and Ca^{2+} facilitates opening in a nearly voltage-independent manner, indicating that Ca^{2+} and voltage sensor activation have energetically additive effects on opening (Cui and Aldrich, 2000; Horrigan and Aldrich, 2002). The transmembrane domain of BK channels, like voltage-gated K^+ (Kv) channels, includes an S5–S6 pore domain and a charged S1–S4 voltage sensor (Ma et al., 2006). Coupling between the voltage sensor and pore can occur presumably as in Kv channels, via interactions within the transmembrane domain (Fig. 1 A) (Lu et al., 2002; Long et al., 2005b). In addition, BK channels contain a large C-terminal cytosolic domain that interacts with intracellular ligands and is directly attached to the S6 activation gate. The cytosolic domain of each α-subunit contains two putative RCK (regulator of K^+ conductance) homology domains (RCK1, RCK2), like those in the prokaryotic channel MthK (Jiang et al., 2001). In MthK, RCK domains from different subunits assemble into a gating ring structure that expands upon Ca^{2+} binding to pull open the gate (Fig. 1 B) (Jiang et al., 2002; Ye et al., 2006), suggesting that Ca^{2+} opens BK channels by increasing tension on the RCK1–S6 linker (Niu et al., 2004). Thus models of BK channel structure support that voltage and Ca^{2+} sensors may act independently on the gate (Fig. 1 C) to exert additive effects on steady-state activation.

Given the example of MthK, one might suppose that any ligand binding to the cytosolic domain of the BK

Correspondence to Frank T. Horrigan: horrigan@mail.med.upenn.edu

Abbreviations used in this paper: Kv, voltage-gated K^+; RCK, regulator of K^+ conductance.

channel must act, like Ca^{2+}, to open the gate by pulling on the RCK1–S6 linker. However this is not necessarily the case. Voltage sensors in BK channels, which are absent from MthK, are potentially available to interact with the cytosolic domain, providing an alternative pathway of communication between ligand binding sites and the transmembrane domain. The cytosolic domain of MthK lies close to the transmembrane domain, presents a relatively flat surface toward the membrane, and with a diameter of >70 Å extends laterally far beyond the pore (Fig. 1 B). All of these features, which are presumably necessary to exert lateral force on the gate via short peptide linkers, would also tend to bring the periphery of the gating ring close to the voltage sensor domain in BK channels (Fig. 1 D). Several observations suggest that interactions between cytosolic and voltage sensor domains occur. Ca^{2+} has effects on gating current, consistent with a weak interaction between Ca^{2+} sensors and voltage sensors (Horrigan and Aldrich, 2002). Intracellular heme has a pronounced effect on voltage gating, weakening the allosteric coupling between voltage sensor and gate (Horrigan et al., 2005). Likewise, chemical modification of a native cysteine residue (C430) in the cytosolic domain alters voltage sensor/gate coupling (Zhang and Horrigan, 2005).

Mg^{2+} has effects on BK channel gating that resemble those of Ca^{2+}: increasing P_O, slowing I_K deactivation, and shifting the G_K-V relation to more negative voltages with little change in shape (Shi and Cui, 2001; Zhang et al., 2001). Effects of Mg^{2+} and Ca^{2+} on the half-activation voltage ($V_{0.5}$) are approximately additive and involve different binding sites (Shi et al., 2002; Xia et al., 2002). Consequently, Mg^{2+} has been proposed to act independently of Ca^{2+} but through a similar functional mechanism. Effects of Mg^{2+} on the G_K-V relation can be reproduced by gating schemes that assume Mg^{2+} acts, like Ca^{2+}, to enhance channel opening independent of voltage sensor activation (Shi and Cui, 2001; Zhang et al., 2001; Hu et al., 2006). However, several lines of evidence suggest that Mg^{2+} and Ca^{2+} do not act through identical functional mechanisms. First, high concentrations of Ca^{2+} (>100 μM), which are known to occupy Mg^{2+} binding sites, have effects that differ qualitatively from those of low $[Ca^{2+}]_i$. While 0–100 μM Ca^{2+} produces a nearly voltage-independent increase in $\log(P_O)$, 100–1,000 μM Ca^{2+} increases $\log(P_O)$ in a voltage-dependent manner (Horrigan and Aldrich, 2002). In addition, mutations in the voltage sensor, including R213Q in S4, disrupt Mg^{2+} sensitivity but not Ca^{2+} sensitivity, suggesting that the voltage sensor plays a critical role in Mg^{2+}-dependent activation (Hu et al., 2003). Indeed, recent evidence indicates that Mg^{2+} bound to the cytosolic domain interacts electrostatically with R213 (Yang et al., 2007).

This study examines the functional interaction between Mg^{2+}- and voltage-dependent activation of mSlo1 BK channels. Effects of 0–100 mM Mg^{2+} on the steady-state and kinetic properties of ionic and gating currents were examined over a wide voltage range in WT channels and channels where either the voltage sensor or a putative Mg^{2+}-binding site in the RCK1 domain were mutated. The results show that Mg^{2+} at the RCK1 site acts primarily to strengthen the allosteric coupling of voltage sensor activation to channel opening. Only at high concentrations (>10 mM), involving an additional very low affinity binding site, does Mg^{2+} have direct effects on opening, like Ca^{2+}. Our results together with the proposed electrostatic nature of Mg^{2+}/voltage sensor interaction suggest that Mg^{2+} and the voltage sensor must interact in multiple states to account for the effects of Mg^{2+} on voltage sensor/gate coupling.

MATERIALS AND METHODS

Channel Expression and Molecular Biology

Experiments were performed with the mbr5 clone of the mouse Slo1 gene (*mSlo1*) (Butler et al., 1993) expressed in *Xenopus* oocytes (for I_K) or HEK 293T cells (for gating current). The clone was propagated and cRNA transcribed as described previously (Cox et al., 1997). Oocytes were injected with ~0.5–5 ng of cRNA, incubated at 18°C, and studied 3–7 d after injection. HEK cells were transfected with mSlo1 in an SRα vector using Lipofectamine (GIBCO BRL/Life Technologies Inc.) 2–3 d before recording as described previously (Horrigan and Aldrich, 2002). Site-directed mutagenesis was performed with the QuikChange XL Site-Directed Mutagenesis Kit (Stratagene) and confirmed by sequencing.

Electrophysiology and Data Analysis

Currents were recorded using the patch-clamp technique in the inside-out configuration (Hamill et al., 1981) at 20 ± 1°C. For Ca^{2+} experiments, the external solution contained (in mM) 104 $KMeSO_3$, 6 KCl, 2 $MgCl_2$, 20 HEPES, and the internal solution contained 110 $KMeSO_3$, 6 HCl, 20 HEPES, and 2 EGTA (0 Ca^{2+}) or 5 HEDTA (Ca^{2+} solution). Ca^{2+} was added as $CaCl_2$ and $[Cl^-]_i$ was adjusted to 10 mM with HCl. Free $[Ca^{2+}]$ for the 2 μM Ca^{2+} solution was measured (1.8 μM) with a Ca^{2+} electrode (Orion Research Inc.). For Mg^{2+} experiments, the external solution contained (in mM) 225 KOH, 196 HCl, 2 $MgCl_2$, 10 HEPES, and internal solutions contained 225 KOH, 5 EGTA, 10 HEPES, plus $MgCl_2$ and HCl to obtain the desired $[Mg^{2+}]$ with $[Cl^-]_i$ = 200 mM. 100 mM Mg^{2+} solution contained a total of 100 mM Mg^{2+} for an estimated free $[Mg^{2+}]$ of 96.1 mM. Total Mg^{2+} in other solutions was adjusted to obtain the indicated free $[Mg^2]$ (2, 5, 10, 21 mM) as calculated by MaxChelator (http://www.stanford.edu/~cpatton/maxc.html) (Patton et al., 2004). Since free $[Mg^{2+}]$ was not measured, the purity of $MgCl_2$ and EGTA stocks were assayed by pH-metric titration (Tsien and Pozzan, 1989) against standardized solutions of EDTA and $CaCl_2$, respectively. For gating currents (I_g) the external solution contained 130 tetraethyl ammonium (TEA)-OH, 100 NMDG, 196 HCl, 2 $MgCl_2$, 10 HEPES, and internal solution contained 225 NMDG-MES, 10 HEPES, 5 EGTA, plus $MgCl_2$ and HCl as above. The pH of all solutions was adjusted to 7.2 with $MeSO_3$. Internal solutions contained 40 μM (+)-18-crown-6-tetracarboxylic acid (18C6TA) to chelate contaminant Ba^{2+} (Diaz et al., 1996; Neyton, 1996).

Data were acquired with an Axopatch 200B amplifier (Molecular Devices Corp.) in patch mode with the Axopatch's filter set at 100 kHz. Currents were filtered by an 8-pole Bessel filter (Frequency Device, Inc.) at 50 kHz (I_K) or 20 kHz (I_g) and sampled at

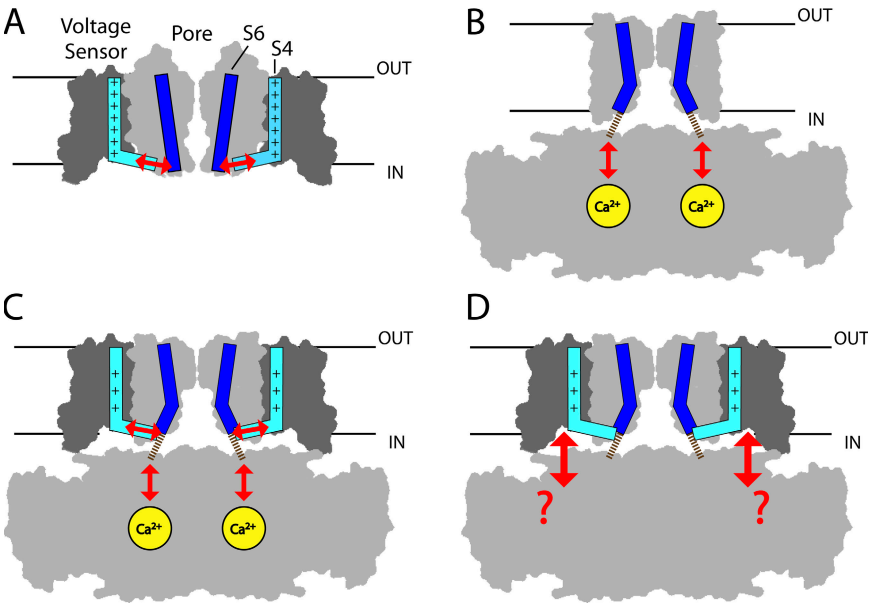

Figure 1. Proposed pathways of sensor/gate interaction for different channels. (A) Kv1.2, where the charged S4 segment (light blue) in the voltage sensor is proposed to interact with the S6 activation gate (dark blue) in the pore via the S4–S5 linker (arrows). The outlines of the S1–S4 voltage sensor domain and S5–S6 pore domain for two subunits from the Kv1.2 crystal structure (Long et al., 2005a) are shown in dark and light gray, respectively, and are truncated at S1 (protein data bank code 2A79). (B) MthK, where Ca^{2+} binding to the cytosolic domain is proposed to cause a conformational change that pulls open the gate through short peptide linkers (dashed lines) that are unresolved in the crystal structure (Jiang et al., 2002) (protein data bank code 1LNQ). The attachment points of the linker on the cytosolic domain (in foreground and background) have been altered to better illustrate that linkers are pulled away from the pore axis. (C) A hypothetical BK channel structure formed by appending the Kv1.2 voltage sensors to MthK shows how Ca^{2+} and voltage may both interact with the gate to have independent effects on activation. The position of the voltage sensors was determined by superimposing the pore domains of Kv1.2 (residues 341–406) and MthK (residues 26–91) in PyMol (http://www.pymol.org). (D) The hypothetical BK channel structure also illustrates the possibility that the large cytosolic domain may interact directly with voltage sensors.

200 kHz with an 18-bit A/D converter (Instrutech ITC-18). For gating currents, the voltage command was also filtered at 20 kHz. A p/4 protocol was used for leak subtraction (Armstrong and Bezanilla, 1974) with a holding potential of −80 mV. Electrodes were made from thick-walled 1010 glass (World Precision Instruments, Inc.) and their tips coated with wax (KERR Sticky Wax). The electrode's resistance in the bath solution (0.5–1.5 MΩ) was used as an estimate of series of resistance (R_S) for correcting the voltage at which macroscopic I_K was recorded. Series resistance error was <15 mV for all data presented. A Macintosh-based computer system was used in combination with Pulse Control acquisition software (Herrington and Bookman, 1995) and Igor Pro for graphing and data analysis (WaveMetrics, Inc.). A Levenberg-Marquardt algorithm was used to perform nonlinear least-squared fits. Data are presented as mean ± SEM.

Open probability (P_O) was estimated by recording macroscopic I_K when P_O was high (≥0.005–0.05) and unitary currents in the same patch when P_O was low (≤0.01–0.1). Macroscopic conductance (G_K) was determined from tail currents at −80 mV following 50-ms voltage pulses, and was normalized by G_{Kmax} to estimate P_O. G_{Kmax} was measured in 5–100 mM Mg^{2+} (0 Ca^{2+}) at V > 200 mV from tail currents and was estimated at $[Mg^{2+}] < 5$ mM as G_{Kmax} (10 Mg^{2+}) $\{\gamma_K([Mg^{2+}])/\gamma_K(10\ Mg^{2+})\}$ where $\gamma_K([Mg^{2+}])$ is the single channel conductance at −80 mV and is reduced slightly (~5%) in 10 Mg^{2+} due to Mg^{2+} block. At more negative voltages, NP_O was determined from steady-state recordings of 1–60 s duration that were digitally filtered at 5 kHz. NP_O was determined from all-points amplitude histograms by measuring the fraction of time spent (P_K) at each open level (K) using a half-amplitude criteria and summing their contributions $NP_o = \Sigma k P_k$. P_O was then determined by estimating N from G_{Kmax} ($N = G_{Kmax}/\gamma_K$, where γ_K is the single channel conductance at −80 mV). Mean activation charge displacement ($q_a = kT\ d(\ln(P_O)/dV)$ was measured from the slope of the $\ln(P_O)$-V relation by linear regression over 60-mV intervals and plotted against mean voltage. Fits of the q_a-V relation were similarly determined by linear regression of simulated data (Ma et al., 2006).

Patch-to-patch variation in $V_{0.5}$ of the G-V and Q-V relationships are observed for Slo1 channels (Stefani et al., 1997; Horrigan et al., 1999). To compensate for the effect of such variation on mean P_o-V and Q_G-V relations, $V_{0.5}$ was determined for each patch and individual relations were shifted along the voltage axis by $\Delta V_{0.5} = (<V_{0.5}> - V_{0.5})$ before averaging, where $<V_{0.5}>$ is the mean for all experiments at the same $[Mg^{2+}]$. Patch to patch variation in P_O at extreme negative voltages is also observed (Horrigan et al., 1999). Therefore, mean $\log(P_O)$-V and τ_K-V relations for 0, 10, and 100 mM Mg^{2+} were constructed using only experiments in which both Mg^{2+} data and matching 0 Mg^{2+} controls exist. In this way, mean relations accurately reflect effects of Mg^{2+} that were observed in individual experiments.

Gating capacitance (C_g) was measured using admittance analysis as previously described (Horrigan and Aldrich, 1999). In brief, gating currents were recorded in response to 0.5-s voltage ramps upon which a sinusoidal voltage command (781 hz, 60 mV peak to peak) was superimposed. Admittance was calculated for each cycle of the sinewave, and capacitance was determined after correcting for phase shifts due to instrumentation.

RESULTS

Mg^{2+} and Ca^{2+} Act through Different Mechanisms

The effects of millimolar $[Mg^{2+}]_i$ and micromolar $[Ca^{2+}]_i$ on steady-state activation are compared in Fig. 2. In addition to increasing open probability, intracellular Mg^{2+} rapidly blocks the pore in a voltage-dependent manner that effectively reduces single channel conductance at depolarized voltages (Ferguson, 1991). Both of these effects are evident by comparing macroscopic potassium currents (I_K) in the presence and absence of 10 mM Mg^{2+} (Fig. 2 A). I_K was evoked by 50-ms pulses to different voltages in inside-out patches from *Xenopus* oocytes

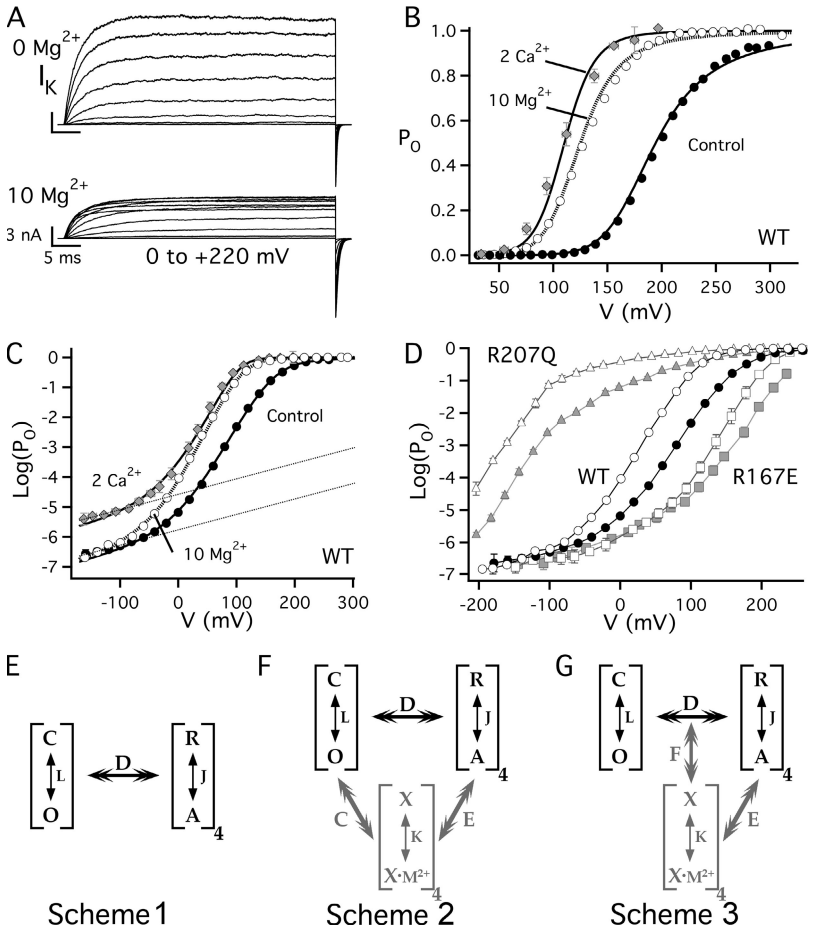

Figure 2. Effects of Mg^{2+} on steady-state activation. (A) Effect of 10 mM Mg^{2+} on macroscopic I_K evoked from mSlo1 channels in response to 50-ms pulses to different voltages in 0 Ca^{2+} from a holding potential of −80 mV. Mg^{2+} decreases outward current at high voltages owing to rapid pore block. However tail currents indicate an increase in P_O and slowing of channel deactivation. (B) Mean normalized G_K-V relations ($P_o = G_K/G_{Kmax}$) determined from tail currents in 10 mM Mg^{2+} (O), 2 μM Ca^{2+} (◆) or the absence of divalent cations (control, ●). (C) Mean log(P_O)-V relations corresponding to B achieve a weakly voltage-dependent limiting slope at extreme negative voltages, indicating that voltage sensors are in the resting state. Dotted lines are exponential fits to control and Ca^{2+} data with partial charge $z_L = 0.3e$ (Ma et al., 2006). (D) Voltage sensor mutations R207Q (△, ▲) and R167E (□, ■) shift both the voltage dependence of activation and Mg^{2+} sensitivity (0 Mg: filled symbols; 10 mM Mg^{2+}: open symbols) relative to the WT (O, ●), implying that Mg^{2+} action depends on voltage sensor activation and is not intrinsically voltage dependent. (E) Voltage-gating mechanism (Scheme 1). Channels undergo a closed–open (C-O) conformational change that is allosterically regulated by four independent and identical voltage sensors that can undergo a resting-activated (R-A) transition. L and J are voltage-dependent equilibrium constants ($L = L_0\exp(z_L V/kT)$, $J = J_0\exp(z_J V/kT) = \exp(z_J[V - V_{hC}]/kT)$) and D is an allosteric factor. (F) Scheme 2 includes a ligand-binding transition (X-X·M^{2+}) in each subunit that allosterically regulates channel opening and voltage sensor activation as described by factors C and E, respectively. Solid curves in B and C represent a fit of this model to Ca^{2+}-dependent activation in 0–100 μM Ca^{2+} (Horrigan and Aldrich, 2002) (V_{hC} = 156 mV, $z_J = 0.58e$, $L_0 = 1.06 \times 10^{-6}$, $z_L = 0.3e$, $K_D(Ca^{2+})$ = 11 μM, C = 8, D = 24.4, E = 2.4). The same model with identical values of V_{hC}, z_J, L_0, z_L, D, and E can fit the Mg^{2+} data (dotted curves) if Mg^{2+} binding is assumed to be voltage dependent (i.e., $K_D(Mg^{2+}) = K_D(0)\exp(-V\gamma 2e/kT)$) ($K_D(0)$ = 9.35 mM, γ = 0.2, C = 1.66) (G) Scheme 3 assumes that ligand binding allosterically regulates voltage/sensor gate coupling and voltage sensor activation as described by allosteric factors F and E, respectively.

expressing mSlo1 BK channels. Mg^{2+} decreases outward current at the most positive voltages owing to pore block, but increases tail currents at −80 mV, indicating that P_O is increased. Normalized G_K-V relations, determined from tail currents exhibit a −67.2 ± 4.9 mV shift in half-activation voltage ($V_{0.5}$) in response to 10 mM Mg^{2+}, with little change in shape, similar to the effect of 2 μM Ca^{2+} (Fig. 2 B).

Despite similar effects of Mg^{2+} and Ca^{2+} on the G_K-V relation, fundamental differences in the action of these ligands are evident when P_O is plotted on a log-scale versus voltage (Fig. 2 C). P_O was measured to values as low as $\sim 10^{-7}$ by recording unitary current activity in macropatches containing hundreds of channels. Log(P_O) is increased by 2 μM Ca^{2+} in a nearly voltage-independent manner, shifting the entire log(P_O)-V curve upward by 1.2 log units (a 15-fold increase in P_O) until channels are maximally activated at positive voltages. P_O is increased 15-fold even at extreme negative voltages (≤−100 mV) where voltage sensors are not activated and log(P_O) is weakly voltage dependent (Fig. 2 C, dotted lines) (Horrigan and Aldrich, 2002). By contrast, 10 mM Mg^{2+} has no effect on steady-state activation at extreme negative voltages and increases log(P_o) in a voltage-dependent manner from −80 to +40 mV such that the effects of Mg^{2+} and Ca^{2+} are similar only at more positive voltages.

Why Is the Effect of Mg^{2+} Voltage Dependent?

Two different mechanisms could potentially account for the voltage dependence of Mg^{2+} action; the effect of Mg^{2+} could depend on the activation state of the voltage sensor, or Mg^{2+} binding could be intrinsically voltage dependent. Voltage-dependent binding must be considered because if Mg^{2+} interacts with the voltage sensor it could also lie within the membrane electric field; and a model assuming that Mg^{2+} traverses a fraction of the electric field (γ = 0.2) to reach its binding site can reproduce the effect of 10 mM Mg^{2+} (Fig. 2, B and C, dotted curves, see legend for details). However, the effects of Mg^{2+} on two voltage sensor mutants (R207Q, R167E)

in Fig. 2 D indicate that voltage sensor activation is critical to the effect of Mg^{2+} and probably sufficient to account for the voltage dependence of Mg^{2+} action.

R207Q in S4 and R167E in S2 shift voltage sensor activation to more negative and positive voltages, respectively (Ma et al., 2006), such that $\log(P_O)$-V relations for these mutants are shifted along the voltage axis relative to the WT in 0 Mg^{2+} (Fig. 2 D, filled symbols). R207Q also shifts the Q-V relation by more than −250 mV, based on gating current measurements, such that even at −200 mV a significant fraction (∼0.2) of voltage sensors are activated (Ma et al., 2006). Both R207Q and R167E are readily activated by 10 mM Mg^{2+} at depolarized voltages (Fig. 2 D), suggesting these mutations do not disrupt Mg^{2+} binding nor interactions of Mg^{2+} with the voltage sensor (Hu et al., 2003; Yang et al., 2007). However the voltage dependence of Mg^{2+}-dependent activation for the mutants is greatly altered relative to the WT, suggesting that Mg^{2+} action depends on the activation state of the voltage sensor. In the case of R167E, Mg^{2+} has no effect on P_O at voltages up to +60 mV where the WT is strongly activated by Mg^{2+}. Conversely, R207Q exhibits a robust 30-fold increase in P_O at negative voltages (−120 to −200 mV) where the WT appears insensitive to Mg^{2+}. The response of R207Q indicates that Mg^{2+} is capable of occupying its binding site even at extreme negative voltages. Thus, it is unlikely that Mg^{2+} binding is intrinsically voltage dependent; and the inability of the WT to be activated at negative voltages likely reflects that Mg^{2+} is incapable of increasing P_O when voltage sensors are in the resting state. This hypothesis is supported by comparison of the WT and R167E data that show that channels are Mg^{2+} insensitive when P_O is weakly voltage dependent.

Understanding the Action of Mg^{2+} in Terms of Allosteric Mechanisms

To determine how Mg^{2+} and voltage sensors interact mechanistically we interpreted our results in terms of a well-established allosteric gating scheme that accounts for the effects voltage on steady-state activation of BK channels (Fig. 2 E, Scheme 1) (Horrigan and Aldrich, 1999; Horrigan et al., 1999). Scheme 1 asserts that the opening of the gate can be described as a concerted, weakly voltage-dependent transition between an open and closed conformation (C-O) with zero-voltage equilibrium constant L_0 and partial charge z_L. In addition, voltage sensors in each of four independent and identical subunits can undergo a transition between a resting and activated conformation (R-A) characterized by equilibrium constant J_0 and partial charge z_J. The coupling between voltage sensor and gate is described by an allosteric factor D, such that the C-O equilibrium constant increases D-fold for each voltage sensor activated and the voltage sensor equilibrium increases D-fold when the channel opens.

Based on Scheme 1 there are four distinct mechanisms by which a ligand might alter P_o. Ligand binding could (a) influence the intrinsic stability of the gate (L_0), (b) perturb the voltage sensor equilibrium (J_0), (c) alter voltage sensor/gate coupling (D-factor), or (d) alter the gating charge associated with voltage sensor activation (z_J) or channel opening (z_L). The action of Ca^{2+} is mainly accounted for by an effect on the gate (L_0) with a minor impact on voltage sensor activation (J_0). This mechanism can be represented by an allosteric model (Fig. 2 F, Scheme 2) that successfully reproduces the effects of Ca^{2+} (Fig. 2, B and C, solid lines) in terms of a ligand-binding equilibrium ($X\text{-}X\cdot M^{2+}$) and allosteric factors C and E that describe the coupling of Ca^{2+} sensors to the gate and to voltage sensors, respectively (Horrigan and Aldrich, 2002). Direct coupling between Ca^{2+} sensors and gate is evident from the ability of Ca^{2+} to increase P_O whether or not voltage sensors are activated. Thus the insensitivity of P_O to 10 mM Mg^{2+} when voltage sensors are in the resting state rules out a similar interaction between Mg^{2+} sensors and gate and indicates that L_0 is unchanged, but leaves open the possibility that Mg^{2+} affects voltage sensor activation or coupling (Fig. 2 G, Scheme 3) or charge.

Mg^{2+} Has Little Effect on Voltage Sensor Activation when Channels Are Closed

To characterize effects of Mg^{2+} on the voltage sensor we recorded gating current from WT and mutant channels (Fig. 3). The results indicate that Mg^{2+} has little effect on the voltage sensor equilibrium (J_0) or gating charge (z_J).

Voltage sensor activation in BK channels is much faster than channel opening (Stefani et al., 1997; Horrigan and Aldrich, 1999). Therefore ON gating current (I_{gON}) reflects primarily voltage sensor activation when channels are closed. Fig. 3 A shows the effects of Mg^{2+} on I_{gON} evoked by brief 0.5-ms depolarizations to +200 mV. 10 mM Mg^{2+} causes an ∼20% increase in peak I_{gON} with little change in kinetics (Fig. 3 A, top). Application of 100 mM Mg^{2+}, to activate very low affinity binding sites (Hu et al., 2006), produces a greater increase in peak current (Fig. 3 A, bottom). Mean charge–voltage relations for closed channels (Q_C-V), determined from I_{gON} (see Fig. 3 legend) are shifted to more negative voltages by -16.7 ± 2.3 mV ($n = 5$) or -29.6 ± 2.6 mV ($n = 3$) in 10 or 100 mM Mg^{2+}, respectively (Fig. 3 B). This shift in half-activation voltage (V_{hC}) occurs without appreciable change in the shape of the Q_C-V relation, suggesting that Mg^{2+} does not alter gating charge. Similarly, effects of 10 mM Mg^{2+} on the time constant of I_{gON} (τ_{gFast}) for a single experiment (Fig. 3 C) reflect a small −21 mV shift in the τ_{gFast}-V relation to more negative voltages.

To better quantify small changes in V_{hC} (ΔV_{hC}) by Mg^{2+} we examined gating capacitance (C_g) (Fig. 3, D–F). C_g is the voltage-dependent component of membrane capacitance and reflects the derivative of gating

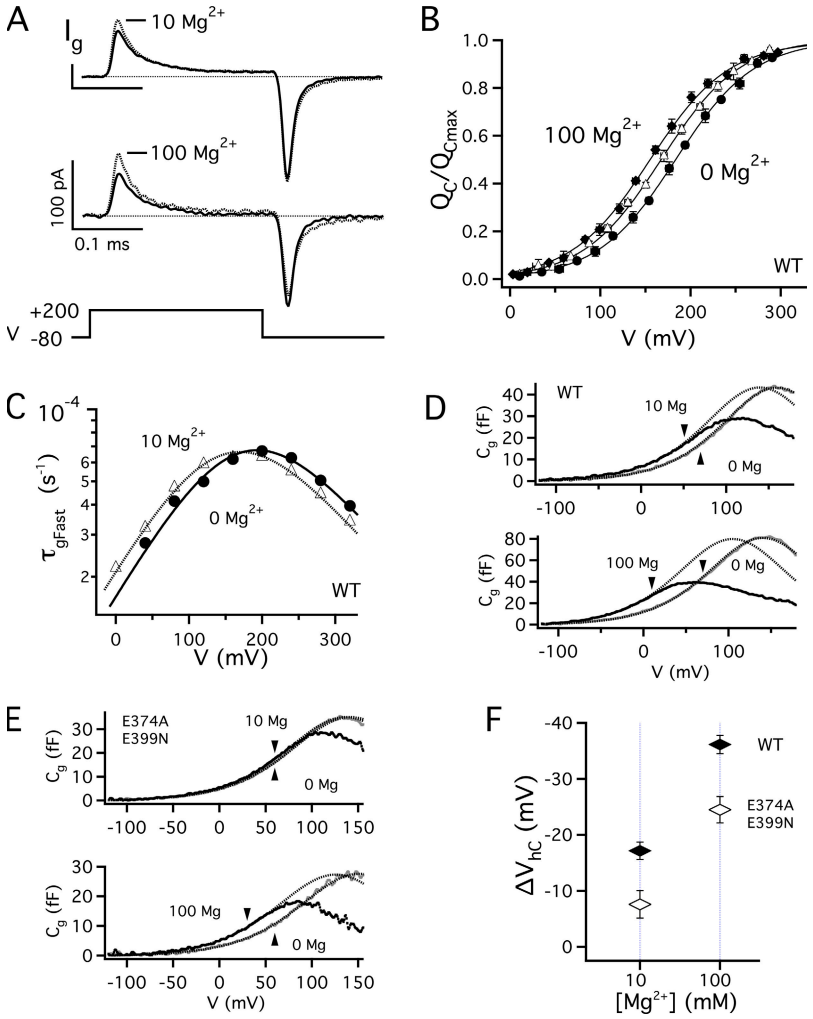

Figure 3. Effects of Mg^{2+} on gating current were measured in the absence of permeant ions and presence of extracellular tetraethyl ammonium (TEA) to block the pore. (A) I_g evoked by 0.5-ms pulses to +200 mV in the presence (dotted traces) or absence (solid traces) of Mg^{2+}, from two different patches testing the effects 10 or 100 mM Mg^{2+}. (B) Mean Q_C-V relations in 0 (●), 10 (△), and 100 (◆) mM Mg^{2+} are fit by Boltzmann functions with identical equivalent charge (z_J = 0.58*e*) (Horrigan and Aldrich, 2002) and were normalized by the fit amplitude (Q_{cMax}). Q_C represents the charge distribution for closed channels, determined by fitting the initial 50–100-μs decay of I_{gON} with an exponential function with time constant τ_{gFast} and integrating the area under the rising phase and fit (Horrigan and Aldrich, 1999). (C) τ_{gFast}-V relations for the patch in A are shifted by −21 mV in 10 mM Mg^{2+}. Relations are fit by functions of the form $\tau_{gFast} = [\alpha(V) + \beta(V)]^{-1}$ where α and β are forward and backward rate constants for voltage sensor activation (0 Mg: $\alpha(0) = 58600\ s^{-1}$, $\beta(0) = 1930\ s^{-1}$; 10 Mg: $\alpha(0) = 45400\ s^{-1}$, $\beta(0) = 2350\ s^{-1}$) ($z_\alpha = 0.3\ e$, $z_\beta = -0.2e$). Representative C_g-V relations obtained with admittance analysis for (D) WT or (E) E374A/E399N channels in the presence (black curves) and absence (gray curves) of 10 or 100 mM Mg^{2+} are fit by the derivative of a Boltzmann function with respect to voltage (dotted curves) with identical amplitude and charge (z_J = 0.58*e*). Shifts along the voltage axis indicate the change in V_{hC} (ΔV_{hC}). Arrows indicate the upper voltage limit of the fit that was determined over a range where most channels are closed ($P_o < 0.1$). (F) $\Delta V_{hC} = [V_{hC}(Mg^{2+}) - V_{hC}(0\ Mg^{2+})]$ for WT (◆, $n = 6$) and E374A/E399N (◇, $n = 4$) determined from C_g-V relations.

charge with respect to voltage. The C_g-V relation was determined from admittance analysis by measuring I_g evoked by a sinusoidal voltage command superimposed on a 500-ms voltage ramp from −200 to +200 mV (see Materials and methods) (Horrigan and Aldrich, 1999, 2002). At voltages where steady-state P_O is low (<0.1), the C_g-V relation approximates the derivative of Q_C-V (Horrigan and Aldrich, 1999). Thus ΔV_{hC} can be determined directly from shifts in the foot of C_g-V relation (Fig. 3 D). Because C_g-V is determined rapidly and with high voltage resolution, small V_{hC} shifts are detectable, the effects of applying and washing out Mg^{2+} can be assessed rapidly, and errors in ΔV_{hC} due to slow changes in V_{hC} from channel oxidation or electrode potential drift are minimized. C_g-V analysis for the WT (Fig. 3 D) yielded ΔV_{hC} values (10 Mg: 17.2 ± 1.5 mV [$n = 6$], 100 Mg: 36.1 ± 1.6 mV [$n = 6$]) similar to those determined from Q_C-V relations.

The effect of Mg^{2+} on V_{hC} is comparable to that of micromolar Ca^{2+} (Horrigan and Aldrich, 2002), consistent with a weak interaction between Mg^{2+} binding and voltage sensor activation in closed channels that increases the voltage sensor equilibrium constant J_0 (e.g., E-factor in Schemes 2 and 3, Fig. 2, F and G). However, millimolar Mg^{2+} may also shift voltage-dependent parameters by nonspecific mechanisms such as screening of membrane surface charge (Hu et al., 2006). Therefore, to assess the impact of the RCK1 Mg^{2+} site on J_0 we compared effects of Mg^{2+} on the WT channel to those of a mutant (E374A/E399N) whose RCK1 site is disrupted (Shi et al., 2002; Hu et al., 2006). This mutation of putative Mg^{2+}-coordinating residues, which reduces the G_K-V shift in 10 mM Mg^{2+} by 80% to −14.0 ± 2.0 mV, also reduces effects of 10 or 100 mM Mg^{2+} on the C_g-V relation (Fig. 3, E and F). The difference in ΔV_{hC} between the WT and mutant ($\Delta\Delta V_{hC} = \Delta V_{hC}$(E374A/E399N) − ΔV_{hC}(WT)) was −9.5 ± 2.8 mV and −11.6 ± 2.8 mV for 10 and 100 Mg^{2+}, respectively, likely representing the effect of RCK1 site occupancy on J_0. The similar impact of mutation in 10 and 100 mM Mg^{2+} is consistent with the expectation that the RCK1 site is nearly saturated in 10 mM Mg^{2+} (Hu et al., 2006).

The small effect of Mg^{2+} on gating current suggests that Mg^{2+} enhances voltage sensor/gate coupling (D).

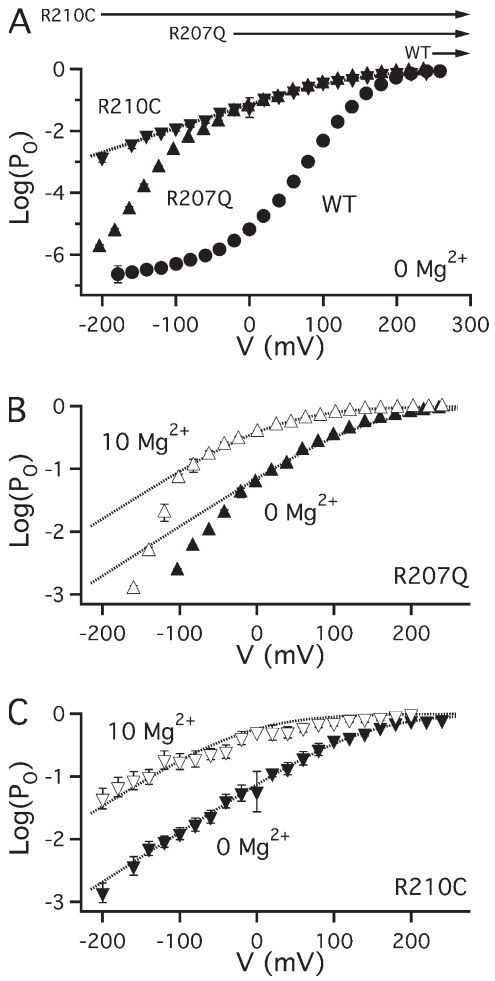

Figure 4. Mg^{2+} facilitates opening in a voltage-independent manner when voltage sensors are constitutively activated. (A) Mean log(P_O)-V relations for WT (●), R207Q (▲), and R210C (▼) in 0 Mg^{2+}. Arrows indicate the voltage range where voltage sensors of WT, R207Q, and R210C are fully activated (see text). Dotted curve represents a Boltzmann fit to R210C with partial charge z = 0.46*e* that describes the weak voltage dependence of channel opening in both mutants when voltage sensors are fully activated (Ma et al., 2006). (B) Mean log(P_O)-V relations for R207Q show that 10 mM Mg^{2+} (△) increases P_O even when voltage sensors are fully activated. Dotted Boltzmann fits from −20 to +240 mV have identical charge (0.46*e*) but $V_{0.5}$ is shifted by −91.6 mV in Mg^{2+}, consistent with a 8.2-fold increase in the C-O equilibrium constant. (C) Mean log(P_O)-V relations for R210C show that 10 mM Mg^{2+}(▽) increases the C-O equilibrium constant in a voltage-independent manner when voltage sensors are constitutively activated. Boltzmann fits have identical charge (0.46*e*) but $V_{0.5}$ is shifted by −122 mV in Mg^{2+}, consistent with a 16.6-fold increase in the C-O equilibrium constant and a twofold increase in the allosteric coupling factor D.

The −17.2 mV ΔV_{hC} by 10 mM Mg^{2+} (Fig. 3 F) can account for a similar G_K-V shift but is much too small to explain the observed −67-mV shift (Fig. 2 B). By contrast, an increase in the coupling factor D can shift $V_{0.5}$ without affecting V_{hC}. In addition, enhanced coupling should facilitate channel opening when voltage sensors are fully activated and facilitate voltage sensor activation when channels are open. These predictions are confirmed below by results in Figs. 4 and 5.

Mg^{2+} Facilitates Opening When Voltage Sensors Are Constitutively Activated

Voltage sensor/gate coupling defines the extent to which P_O is increased by voltage sensor activation. According to Scheme 1, the C-O equilibrium constant increases from L_0 when voltage sensors are in the resting state to L_0D^4 when all four voltage sensors are activated. If 10 mM Mg^{2+} enhances coupling (D) without affecting L_0, then the C-O equilibrium constant when voltage sensors are fully activated should increase by a factor of δD^4 where $\delta D = D(Mg^{2+})/D(\text{control})$. This predicted facilitation of opening cannot be tested for the WT channel because in 0 Mg^{2+} P_O is already nearly saturated (∼1) at potentials >250 mV where voltage sensors are fully activated (compare G_K-V in Fig. 2 B and Q_c-V in Fig. 3 B). However, facilitated opening by Mg^{2+} can be observed in mutants with enhanced voltage sensor activation (R207Q, R210C; Fig. 4).

Fig. 4 A compares the log(P_O)-V relations for WT, R207Q, and R210C channels in 0 Mg^{2+}. R207Q shifts Q_C-V, as noted above, such that this relation is saturated and voltage sensors are fully activated at V ≥ −20 mV (Ma et al., 2006) (Fig. 4 A, labeled arrow). Over this voltage range, P_O is weakly voltage dependent and well described by a Boltzmann function (dotted curve) as expected for channels with fully activated voltage sensors undergoing a two-state C-O transition with equilibrium constant L_0D^4 (Horrigan and Aldrich, 2002). Importantly, the weak voltage dependence of L_0 reduces P_O to nonsaturating levels at potentials where the mutant voltage sensors are still fully activated (e.g., P_O = 0.04 at −20 mV). The P_O-V relation for R210C is indistinguishable from that of R207Q at V ≥ −20 but extends the weakly voltage-dependent phase of P_O to less than −200 mV, suggesting that R210C voltage sensors are constitutively activated (Ma et al., 2006). The difference between WT and R207Q in Fig. 4 A is consistent with a 100-fold change in the voltage sensor equilibrium constant J_0 (Horrigan and Aldrich, 1999; Ma et al., 2006) and illustrates qualitatively the effect expected if Mg^{2+} acts merely to promote voltage sensor activation. That is, an increase in J_0 can shift the steepest part of the log(P_O)-V relation to more negative voltages but cannot increase P_O above the limiting relation defined by L_0D^4 (Fig. 4 A, dotted curve). By contrast, 10 mM Mg^{2+} markedly increases P_O for R207Q (Fig. 4 B) and R210C channels (Fig. 4 C) when voltage sensors are fully activated, indicating that L_0D^4 is increased. This increase presumably reflects enhanced voltage sensor/gate coupling (increased D) because L_0, although it cannot be measured directly for R207Q or R210C channels, is insensitive to 10 mM Mg^{2+} in WT and R167E (Fig. 2 D).

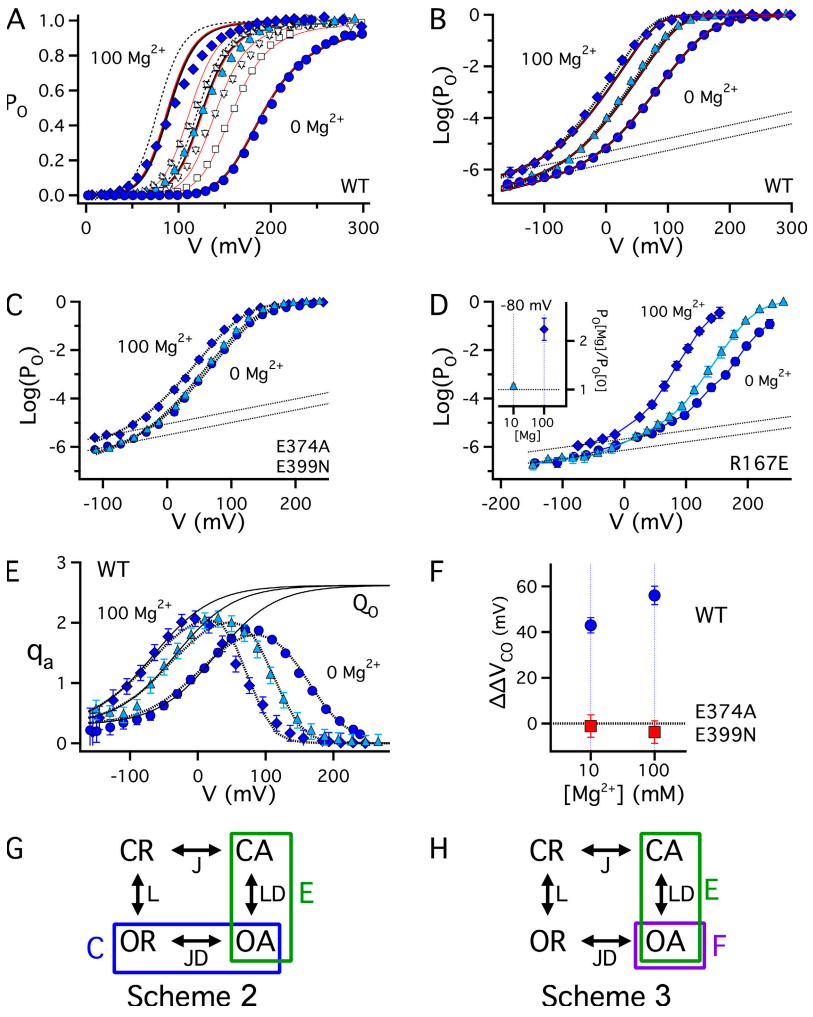

Figure 5. Effects of Mg^{2+} on different binding sites were determined by measuring P_O for WT and mutant channels in 0–100 mM Mg^{2+} (0, blue circle; 2, □; 5, ▽; 10, blue triangle; 21, ◺; 100, blue diamond, mM Mg^{2+}). (A) Normalized mean G_K-V relations for the WT in 0–100 mM Mg^{2+}. (B) Mean $\log(P_O)$-V relations for WT in 0, 10, and 100 mM Mg^{2+} reveal that 100 Mg^{2+} increases P_O at extreme negative voltages. These plots represent the same data as in A but were averaged in 20 mV rather than 10-mV bins to match the voltage interval for low P_O measurements. Dotted lines are exponential fits to P_O at extreme negative voltages in 0 and 100 Mg^{2+} with partial charge $z_L = 0.3e$. (C) Mean $\log(P_O)$-V relations in 0, 10, and 100 mM Mg^{2+} for E374A/E399N show that mutation of the putative Mg^{2+} site in RCK1 almost abolishes effects of 10 mM Mg^{2+} but leaves the P_O increase by 100 Mg^{2+} (dotted lines) intact. (D) Mean $\log(P_O)$-V relations in 0, 10, and 100 mM Mg^{2+} for R167E achieve a limiting slope at more positive voltages than the WT, confirming that P_O is increased by 100 Mg^{2+} when voltage sensors are in the resting state (dotted lines). Inset graph plots the ratio of NP_O in the presence and absence of Mg^{2+} at −80 mV from a larger set of experiments. (E) Mean q_a-V relations for the WT in 0, 10, and 100 mM Mg^{2+} were derived from the slope of $\log(P_O)$-V in B (see text). Solid curves are estimates of the Q_O-V relation determined by fitting the foot of the q_a-V relation (to ~80% of peak q_a) with a function $q_a = z_L + 4z_J [1 + \exp([V_{hO} - V]z_J/kT)]^{-1}$ where $z_L = 0.3e$, $z_J = 0.58e$, and $V_{hO} = 26.5 \pm 2.1$, -33.6 ± 2.4, -65.6 ± 3.7 mV in 0, 10, and 100 mM Mg^{2+}, respectively. (F) Plot of $\Delta\Delta V_{CO} = \Delta V_{hC} - \Delta V_{hO}$ for 10 and 100 mM Mg^{2+} in WT (blue circle) and E374A/E399N (red square) channels where $\Delta V_{hO} = [V_{hO}(Mg^{2+}) - V_{hO}(0\ Mg^{2+})]$ was estimated from the q_a-V relation as in E and ΔV_{hC} was determined from gating current (Fig. 3 F). Nonzero values of $\Delta\Delta V_{CO}$ indicate that Mg^{2+} alters voltage sensor/gate coupling in the WT. However, effects on coupling are abolished by the E374A/E399N mutation. (G) Alternative representation of Scheme 2 (Fig. 2 F) shows the four states defined by the voltage sensor and gate conformation in each subunit and the equilibrium constants defined by Scheme 1 (Fig. 2 E). Boxes denote the states stabilized by ligand binding, as defined by allosteric factors C and E. (H) In Scheme 3, the allosteric factor F defines a stabilization of the OA state that alters voltage sensor/gate coupling (allosteric factor D). Dotted curves in A–E represent simultaneous fits to the P_o-V, $\log(P_O)$-V, and q_a-V relations in 0, 10, and 100 mM Mg^{2+} using Scheme 1 (Fig. 2 E) (Table I parameters WT_A, E374A/E399N). Solid black curves in A and B represent an alternative fit to the WT data (WT_B parameters). Red curves in A represent fits to a two-site model (Eq. 2) that assumes each subunit in the WT contains a very low affinity and an RCK1 binding site described by Schemes 2 and 3, respectively (Table II parameters).

Analysis of the mutant data indicate that 10 mM Mg^{2+} produces an approximate twofold increase in the coupling factor D. Fig. 4 C shows that R210C channels are activated by 10 mM Mg^{2+} in a voltage-independent manner, consistent with the assumption that voltage sensors are constitutively activated. Mean $\log(P_0)$-V relations in the presence and absence of Mg^{2+} were fit by Boltzmann functions with identical charge (Fig. 4 C, dotted curves), as expected if Mg^{2+} increases the C-O equilibrium constant by a voltage-independent factor (δD^4) and Mg^{2+} binding is not voltage dependent. A similar response is observed for R207Q at $V \geq -20$ mV (Fig. 4 B, dotted curves). The fits to R207Q and R210C yield δD^4 values of 8.2 and 16.6, respectively, implying a 1.7–2.0-fold increase in D. A more direct estimate of δD^4 is obtained from the Mg^{2+}-dependent increase in P_O for R210C at extreme negative voltage. Over a range of voltages (−200 to −140 mV) where P_O is small (<0.1) and therefore approximates the C-O equilibrium constant, Mg^{2+} increases P_O by an average of 21.6 ± 6.0-fold (δD^4), indicating a 2.16 ± 0.13-fold increase in D, consistent with the Boltzmann fits.

Different Mg^{2+} Sites Have Distinct Effects on Gating

To further characterize the action of Mg^{2+} at both RCK1 and very low affinity binding sites we examined the effects on P_O of different $[Mg^{2+}]_i$, up to 100 mM, in WT and mutant channels (Fig. 5). The RCK1 site with an

estimated K_D of 2.2–5.5 mM should be nearly saturated at 10 mM Mg^{2+}, whereas a putative very low affinity site (K_D: 40–136 mM) is not significantly affected until concentrations >10 mM (Hu et al., 2006). The effects of high and low concentrations of Mg^{2+} appear similar in that G_K-V relations are progressively shifted to more negative voltages with little change in shape (Fig. 5 A) (Shi and Cui, 2001; Zhang et al., 2001; Hu et al., 2006). Increasing Mg^{2+} from 10 to 100 mM shifted the G-V by an additional −34 mV (Fig. 5 A). However, log(P_O)-V relations reveal that 100 mM Mg^{2+} also increases P_O significantly at extreme negative voltages (Fig. 5 B). Thus it appears that occupancy of very low affinity Mg^{2+} sites, unlike the RCK1 site, influence the gate (L_0) to increase P_O when voltage sensors are not activated.

The log(P_O)-V relation in 100 mM Mg^{2+} appears to achieve a limiting slope between −160 and −140 mV, where P_O is increased 2.9-fold relative to the control (Fig. 5 B, dotted lines), implying a 2.9-fold increase in L_0. However measurements below −140 mV were difficult to obtain. Therefore, to confirm that 100 mM Mg^{2+} increases L_0 we also compared log(P_O)-V relations in 0, 10, and 100 mM Mg^{2+} for two mutant channels (Fig. 5, C and D).

Mutation of the RCK1 site (E374A/E399N) largely eliminates the response to 10 mM Mg^{2+} but leaves the P_O increase by 100 mM Mg^{2+} intact (Fig. 5 C). The mutation reduces the G_K-V shift ($\Delta V_{0.5}$) by 10 and 100 Mg^{2+} to −14.0 ± 2.0 mV and −34.6 ± 1.8 mV, respectively, similar to previous reports (Shi and Cui, 2001; Hu et al., 2006). The reduced shift allows log(P_O)-V to achieve a limiting slope at more positive voltages than the WT (Fig. 5 C, dotted lines), indicating a 2.9-fold increase in L_0 with 100 mM Mg^{2+}, like the WT.

The response of E374A/E399N is important not only in verifying that L_0 is increased by 100 mM Mg^{2+} but also in ruling out that Mg^{2+} occupancy of either the RCK1 site or Ca^{2+}-binding sites contribute to L_0. The insensitivity of L_0 to 10 mM Mg^{2+} in the WT could conceivably reflect an ability of Mg^{2+} at the RCK1 site to decrease L_0 that is masked by the action of Mg^{2+} at other sites. However, this possibility is unlikely since L_0 is also insensitive to 10 mM Mg^{2+} in E374A/E399N. In addition this result indicates that high affinity Ca^{2+}-binding sites, which are known to bind Mg^{2+} at millimolar concentrations, are not responsible for the L_0 increase in 100 mM Mg^{2+} because such sites should already be nearly saturated in 10 mM Mg^{2+} (Shi and Cui, 2001; Zhang et al., 2001; Hu et al., 2006). Thus the E374A/E399N results confirm that occupancy of a very low affinity Mg^{2+} site is required to increase L_0.

The R167E mutant was used to better quantify the effects of Mg^{2+} on L_0 (Fig. 5, D and E). R167E is activated strongly by 100 mM Mg^{2+} but achieves a limiting slope at voltages ∼100 mV more positive than the WT (Fig. 5 D, dotted lines). Thus L_0 can be determined at voltages that are sufficiently negative to achieve a limiting slope but not too extreme to prevent steady-state recording. The effects on L_0 of 10 and 100 mM Mg^{2+} were determined from the change in NP_O at −80 mV in patches where Mg^{2+} was repeatedly applied and washed out. The results confirm that 10 mM Mg^{2+} has little or no effect on L_0 (1.06 ± 0.05-fold change, $n = 10$), whereas 100 mM Mg^{2+} increased L_0 by a factor of 2.24 ± 0.23 ($n = 5$) (Fig. 5 D, inset).

Mg^{2+} Enhances Voltage Sensor Activation when Channels Are Open

The voltage dependence of P_O in the WT channel provides further evidence that Mg^{2+} enhances voltage sensor/gate coupling. According to Scheme 1, the equilibrium constant for voltage sensor activation when channels are open (J_0D) is directly proportional to D. Therefore the charge–voltage relation for open channels (Q_o-V), should be shifted to more negative voltages by Mg^{2+} if coupling is enhanced. Although BK channel voltage sensors can move when channels are open, determination of Q_o from gating currents is difficult because channels close rapidly (Horrigan and Aldrich, 1999). However, Q_o can be assessed in a model-independent fashion from the logarithmic slope of the P_o-V relation (Horrigan and Aldrich, 2002). The mean activation charge displacement ($q_a = kT d(ln[P_o])/dV$) exhibits a bell-shaped dependence on voltage that is plotted in Fig. 5 E for 0, 10, and 100 mM Mg^{2+}. q_a is expected to approximate Q_o at voltages where both P_O and Q_c are small (Horrigan and Aldrich, 2002; Ma et al., 2006). Thus the Q_o-V relation is approximated by the foot of the q_a-V relation at negative voltages, and is markedly left-shifted by Mg^{2+}, indicating that voltage sensor activation is enhanced when channels are open.

To estimate the increase in voltage sensor/gate coupling by Mg^{2+} we fit the foot of the mean q_a-V relations with a function predicted by Scheme 1 to describe Q_o: $Q_o = z_l + 4z_J B(V)$, where B(V) is a Boltzmann function with charge z_J and half activation voltage V_{hO} (Fig. 5 E, solid curves). The fits indicate that V_{hO} is shifted by −60 ± 3 mV and −92 ± 4 mV in 10 Mg^{2+} and 100 Mg^{2+}, respectively. Changes in the coupling factor D can be determined by comparing the shift in Q_O (ΔV_{hO}) to that in Q_C (ΔV_{hC}). Q_O depends on both D and J_0, whereas Q_C depends only on J_0. Therefore the quantity $\Delta\Delta V_{CO} = [\Delta V_{hC} - \Delta V_{hO}]$, plotted in Fig. 5 F for WT and E374A/E399N channels, should depend only on D (i.e., $\delta D = \exp(z_J \Delta\Delta V_{CO}/kT)$, based on Scheme 1). Fig. 5 F indicates $\Delta\Delta V_{CO}$ = 43 ± 3 mV in 10 mM Mg^{2+}, corresponding to a 2.7-fold increase in D. 100 mM Mg^{2+} produces a larger $\Delta\Delta V_{CO}$ (56 ± 4 mV), corresponding to a 3.6-fold increase in D, that probably represents the effect of saturating the RCK1 site. $\Delta\Delta V_{CO}$ for the E374A/E399N mutant is not significantly different from 0 ($P < 0.05$, t test) in 10 or 100 Mg^{2+} (Fig. 5 F), implying that all

TABLE I

Scheme 1 Parameters

	WT	WT_A		WT_B		E374A/E399N		
$[Mg^{2+}]$ (mM)	0	10	100	10	100	0	10	100
V_{hC} (mV)	156.2	139.1	120.1	139.1	120.1	142.9	135.3	118.4
$J_0 \times 10^2$	2.77	4.10	6.34	4.10	6.34	3.76	4.47	6.60
$L_0 \times 10^6$	1.06	1.08	2.57	1.08	2.57	1.66	1.31	4.16
D	24.4	52.2	68.8	48	55	25.9	27.7	23.0

Parameters for Eq. 1 that were varied to fit WT and E374A/E399N data in 0–100 mM Mg^{2+} (Fig. 5, A, B, C, and E). V_{hC} in 10 and 100 mM were determined as $V_{hC}(0) + \Delta V_{hC}(Mg^{2+})$ where $V_{hC}(0)$ was determined from the 0 Mg^{2+} fit and $\Delta V_{hC}(Mg^{2+})$ from gating current (Fig. 3 F). J_0 is determined from V_{hC} ($J_0 = \exp(-V_{hC}z_J/kT)$). Charge parameters were fixed ($z_J = 0.58$ *e*, $z_J = 0.30$ *e*).

changes in voltage sensor/gate coupling can be attributed to the RCK1 site.

Modeling the Effects of Mg^{2+} on Steady-State Activation

The above results suggest that 10 mM Mg^{2+} acts primarily at the RCK1 binding site to enhance voltage sensor/gate coupling (D) with a minor effect on the voltage equilibrium (J_0), and that 100 mM Mg^{2+} causes additional increases in D, J_0, and L_0 that reflect action at both RCK1 and very low affinity binding sites. To confirm that these parameter changes are sufficient to describe the effects of Mg^{2+} on steady-state activation and to better quantify the changes in D we fit simultaneously the $\log(P_O)$-V, q_a-V, and P_O-V relations for 0, 10, and 100 mM Mg^{2+} using Scheme 1, as defined by Eq. 1:

$$P_o = \frac{L(1+JD)^4}{L(1+JD)^4 + (1+J)^4}, \quad (1)$$

$$\text{where } L = L_0 e^{\left(\frac{z_L V}{kT}\right)}; \qquad J = J_0 e^{\frac{z_J V}{kT}} = e^{\frac{z_J [V - V_{hC}]}{kT}}$$

The 0 Mg^{2+} data were fit by setting charge parameters to values determined previously ($z_J = 0.58$ *e*, $z_L = 0.3$ *e*) (Horrigan and Aldrich, 2002) and allowing all other parameters (J_0, L_0, D) to vary, yielding results (Table I, WT 0 Mg^{2+}) similar to previous reports (Horrigan and Aldrich, 2002; Ma et al., 2006). To fit the Mg^{2+} data, the change in J_0 relative to 0 Mg^{2+} was set by gating current measurements (ΔV_{hC}, Fig. 3 F), while L_0 and D were allowed to vary. Excellent fits to the $\log(P_O)$-V and q_a-V relations were obtained in this way (Fig. 5, B and E, dotted curves), with 10 Mg^{2+} increasing D by a factor of 2.14, and 100 Mg^{2+} causing a greater increase in D (2.83-fold) together with a 2.43-fold increase in L_0 (Table I, WT_A parameters). A similar procedure was used to fit the E374A/E399N data (Fig. 5 C, dotted curves), yielding values of D (Table I, E374A/E399N parameters) that vary by <15% relative to the control, which is within the resolution of our measurement (Ma et al., 2006). Thus, shifts in V_{hc} determined from gating currents together with an increase in L_0 in 100 Mg^{2+} appear sufficient to account for the changes in $\log(P_O)$-V when the RCK1 site is disrupted.

Although the fits from Scheme 1 reproduced the effects of Mg^{2+} on $\log(P_O)$ and q_a, they overestimated the shift in $V_{0.5}$ especially in 100 Mg^{2+} (Fig. 5 A, dotted curves). $V_{0.5}$ can be fit at the expense of underestimating the shift in the $\log(P_O)$-V relation by reducing the Mg^{2+}-dependent change in D as illustrated by alternative fits in Fig. 5 (A and B, thick solid curves) where D was increased by factors of 1.97 and 2.26 in 10 and 100 mM Mg^{2+}, respectively (Table I, WT_B parameters). These parameters reasonably approximate the 10 Mg^{2+} P_O-V and $\log(P_O)$-V relations but overestimate the steepness of P_O-V in 100 Mg^{2+} (Fig. 5 A). This discrepancy reflects a decrease in the slope of P_O-V as Mg^{2+} is increased from 10 to 100 mM Mg^2, a feature of the data that is not reproduced by Scheme 1.

To account explicitly for the effects of Mg^{2+} binding on the parameters in Scheme 1 we modeled the effects of very low affinity and RCK1 binding sites in terms of Schemes 2 and 3, respectively (Fig. 2, F and G). These allosteric mechanisms assume that Mg^{2+} can bind to any state of the channel defined by Scheme 1 and that effects of Mg^{2+} on the relative stability of different states therefore reflect the relative affinity of Mg^{2+} for these states. This principal is illustrated in Fig. 5 (G and H) by alternative representations of Schemes 2 and 3 that include the four states (CR, OR, CA, OA) and equilibrium constants defined by Scheme 1 for a single subunit, where boxes and associated allosteric factors indicate the states that are stabilized relative to the CR state by ligand binding. In Scheme 2, the action of Mg^{2+} is defined by its dissociation constant for the CR state (K_D) and two allosteric factors (C and E). C defines the increase in affinity associated with channel opening, such that K_D is reduced C-fold for the OR and OA states (Fig. 5 G, labeled box). Likewise, E defines the change in K_D associated with voltage sensor activation (Fig. 5 G, CA and OA states). These changes in affinity can account for effects of Mg^{2+} on the equilibria for channel opening (L_0) and voltage sensor activation (J_0). However, voltage sensor/gate coupling (D) is unchanged in Scheme 2 because the effects of C and E are independent and neither alters binding in a manner that depends on the state of both the voltage sensor and gate. By contrast, in Scheme 3, D

TABLE II

Two-Site Model Parameters

Site (i)	K_{Di}	C_i	E_i	F_i	K_D(CR)	K_D(OR)	K_D(CA)	K_D(OA)
1	5.0		1.35	2.0	5.0	5.0	3.70	1.85
2	70	1.6	2.3		70	43.8	30.4	19.0

Parameters that were varied to fit Mg^{2+} data (Fig. 5, A and B) for WT (Eq. 2) and E374A/E399N (Eq. 2 with $K_1 = 0$). Remaining parameters (z_J, z_L, J_0, L_0, D) were identical to those for 0 Mg^{2+} in Table I. These parameters predict ΔV_{hC} values of −15.7 mV (WT, 10 Mg), −36.9 mV (WT, 100 Mg), −6.5 mV (E374A/E399N, 10 Mg), −24.4 mV (E374A/E399N, 100 Mg); similar to those measured in Fig. 3 F.

is increased F-fold upon ligand binding by assuming that the affinity of the open-activated state (OA) is increased relative to all other states by an allosteric factor F. Scheme 3 also includes an independent effect of voltage sensor activation on Mg^{2+} affinity (E-factor) as in Scheme 2, to account for effects on J_0.

The data in Fig. 5 (A and B) were fit (red curves, Table II parameters) by a two-site model that assumes the channel contains a single RCK1 (site 1, Scheme 3) and a very low affinity (site 2, Scheme 2) binding site in each of four identical subunits, yielding Eq. 2 (see below), where L, J, and D are defined as in Eq. 1; E_1, F_1 and C_2, E_2 are allosteric factors for sites 1 and 2, respectively; and $K_i = [Mg^{2+}]/K_{Di}$ ($i = 1,2$), where K_{Di} is dissociation constant for each binding site in the CR state.

The fits of Eq. 2 to P_O-V and log(P_O)-V relations in 0, 10, and 100 mM Mg^{2+} were almost identical to those obtained with Scheme 1 (Fig. 5, A and B) and predict shifts in V_{hC} for both WT and E374A/E399N (Table II) similar to those measured from gating current (Fig. 3 F). Parameters for site 1 (RCK1) were well constrained by fitting P_O-V relations in 2, 5, 10, and 21 mM Mg^{2+} (Fig. 5 A) and yielded a K_D for the CR state of 5.0 mM (the K_D of other states are indicated in Table II). A small E_1-factor (1.35) was sufficient to explain the ΔV_{hC} attributed to the RCK1 site, whereas a larger F_1-factor of 2.0 was required to explain the enhancement of voltage sensor/gate coupling. The site 2 (very low affinity) parameters were not as well constrained because few concentrations >10 mM were tested and the effect of saturating this site was not determined.

Effects of Mg^{2+} on I_g Kinetics and the Deactivation Pathway

Although gating current is relatively insensitive to Mg^{2+} when channels are closed (Fig. 3), the ability of Mg^{2+} to shift the Q_o-V relation implies that I_g kinetics must be altered when channels are open. Such an effect is evident from OFF gating currents (I_{gOFF}) following pulses of different duration (0.05–20 ms, +200 mV) in 0 and 10 mM Mg^{2+} (Fig. 6 A). Normalized I_{gOFF} traces (Fig. 6 B) show that OFF kinetics following brief pulses (≤0.1 ms, red traces), that are comparable to the delay in I_K activation (Horrigan et al., 1999) and open few channels, are similar in 0 or 10 Mg^{2+}. However, as pulse duration increases and channels open, voltage sensor deactivation is slowed, reflecting that Q_o-V is shifted to more negative voltages than Q_c-V (Horrigan and Aldrich, 1999). The slowing of I_{gOFF} occurs in 0 Mg^{2+} but is more prominent in 10 Mg^{2+} (Fig. 6 B) because Mg^{2+} increases the difference between Q_O and Q_C (Fig. 5 F) and the fraction of channels that open at +200 mV (Fig. 2 B).

To distinguish effects of Mg^{2+} on voltage sensor deactivation kinetics and P_O, OFF kinetics were analyzed by plotting the time course of OFF charge movement (Q_{OFF}) on a semi-log scale (Fig. 6 C) and comparing the effect of brief ("closed") and prolonged ("open") depolarizations. The decay of Q_{OFF} can be described by three exponential components (τ_{Fast}, τ_{Med}, τ_{Slow}) reflecting the predicted pathways of voltage sensor deactivation (Horrigan and Aldrich, 1999). Scheme 1* (Fig. 6 D) is a kinetic scheme that depicts the 10 states and transitions defined by Scheme 1, representing the O and C conformation with zero to four activated voltage sensors. Q_{OFF} following a brief depolarization is well described by a single exponential function (τ_{Fast}) representing the deactivation of voltage sensors in closed channels (C_4 to C_0 transitions in Scheme 1*). Q_{OFF} for open channels is characterized by a component representing the deactivation of voltage sensors when channels are open (Fig. 6 D, Med) and another that is rate limited by channel closing (Fig. 6 D, Slow). Therefore, Q_{OFF} following prolonged depolarizations to +200 mV (0, 10 Mg [open], Fig. 6 C) are well fit by triple exponential functions where the fast component is small because most channels are open. This analysis confirms that voltage sensor deactivation in open channels (τ_{Med}, Fig. 6 C, dotted red lines) is slowed (2.3-fold) by 10 mM Mg^{2+}. In addition τ_{Slow} (Fig. 6 C, solid red lines) is increased 1.5-fold, consistent with a slowing of channel closing by Mg^{2+}.

Further insight into the mechanism of Mg^{2+} action is provided by plotting the amplitude of the three OFF

$$P_o = \frac{L\left[(1+K_1)(1+K_2C_2)+JD(1+K_1E_1F_1)(1+K_2C_2E_2)\right]^4}{L\left[(1+K_1)(1+K_2C_2)+JD(1+K_1E_1F_1)(1+K_2C_2E_2)\right]^4+\left[(1+K_1)(1+K_2)+J(1+K_1E_1)(1+K_2E_2)\right]^4}, \quad (2)$$

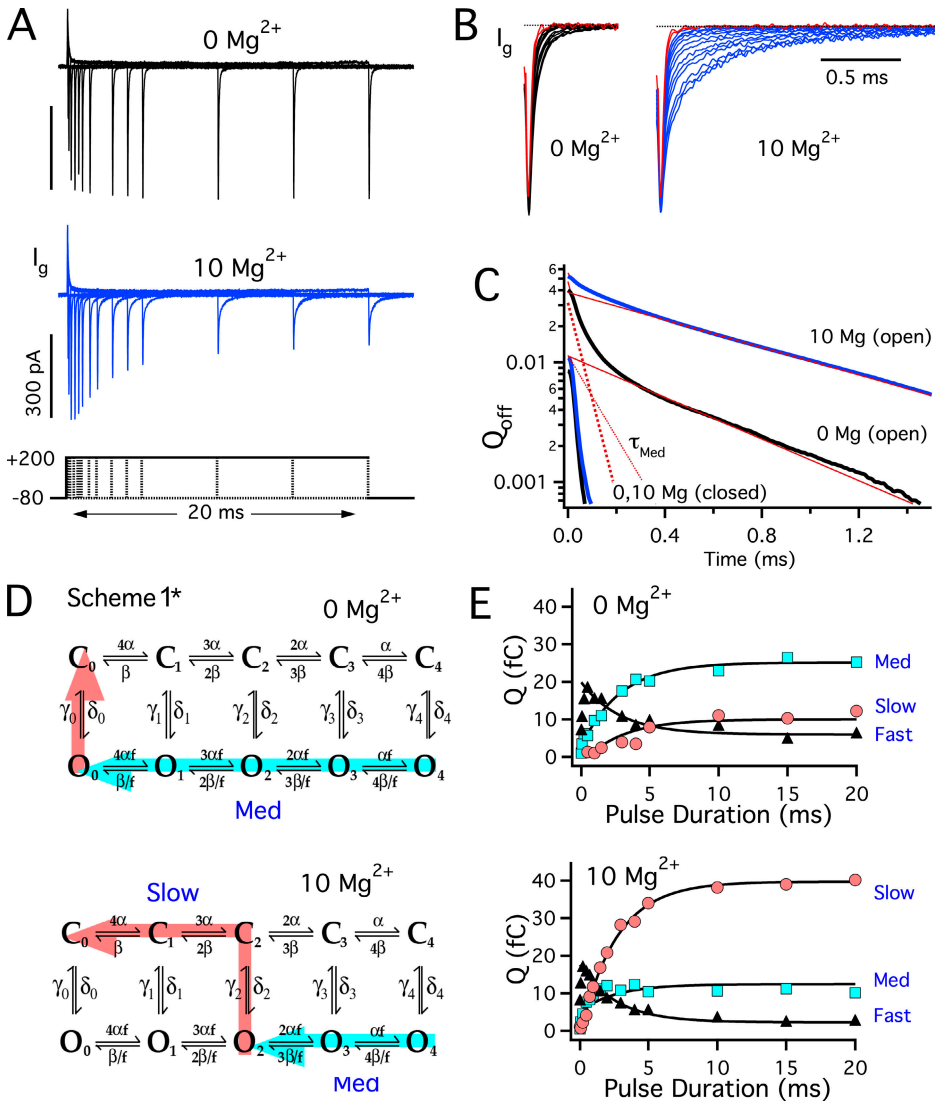

Figure 6. Mg^{2+} affects voltage sensor deactivation when channels are open. (A) I_g evoked by pulses to +200 mV of different duration (0.05–20 ms) in 0 and 10 mM Mg^{2+}. (B) Normalized OFF currents from A decay more slowly as pulse duration increases, especially in the presence of Mg^{2+}. Red traces represent 0.05 and 0.1-ms pulses. (C) OFF kinetics at −80 mV following brief (closed) or prolonged (open) pulses are compared by plotting the quantity $Q = Q_{OFF}(t) - Q_{OFFSS}$ on a log scale vs. time where Q_{OFF} is the integral of I_{gOFF} and Q_{OFFSS} is the steady-state value of $Q_{OFF}(t)$. The "closed" traces, representing the average of 0.05 and 0.1-ms records, have an exponential time course with almost identical kinetics (τ_{Fast}) in 0 Mg^{2+} (15.5 μs) or 10 mM Mg^{2+} (16.3 μs). The "open" traces, representing the average of 10, 15, and 20-ms records, were fit by triple exponential functions (0 Mg^{2+}: q_{Fast} = 6.2 fC, τ_{Fast} = 15.5 μs, q_{MED} = 24.9 fC, τ_{MED} = 54.1 μs, q_{SLOW} = 11.2 fC, τ_{SLOW} = 500 μs; 10 Mg^{2+}: q_{Fast} = 2.6 fC, τ_{Fast} = 16.3 μs, q_{MED} = 10.6 fC, τ_{MED} = 127 μs, q_{SLOW} = 39.1 fC, τ_{SLOW} = 756 μs). The Med and Slow components of the fits are shown as dotted and solid lines respectively. (D) Scheme 1* depicts the five closed (C_i) and open (O_i) states defined by Scheme 1, where i represents the number of activated voltage sensors (i = 0–4). δ_i and γ_i are forward and reverse rate constants for channel opening while α and β are rates for voltage sensor activation when channels are closed, and f = $\sqrt{D}$. Colored arrows represent different pathways of deactivation and Q_{OFF} components for open channels in 0 Mg^{2+} (top) or 10 mM Mg^{2+} (bottom) at −80 mV. In 10 mM Mg^{2+}, channels can close from open states other than O_0 because Mg^{2+} allows voltage sensors in open channels to remain activated at −80 mV (Q_O, Fig. 5 E). The figure illustrates one possible pathway, through the O_2 state. After channels close, voltage sensors can completely deactivate in 10 mM Mg^{2+} (Q_C, Fig. 3 B). This charge movement is limited by the closing rate and therefore contributes to the Slow component of Q_{OFF}. (E) The amplitude of the three OFF components (Fast, ▲; Med, light blue square; Slow, pink circle) for the experiment in A are plotted vs. pulse duration and fit by exponential functions (0 Mg^{2+}, τ = 2.8 ms; 10 Mg^{2+}, τ = 2.6 ms).

components (Q_{Fast}, Q_{Med}, Q_{Slow}) versus pulse duration (Fig. 6 E). As pulse duration increases, Q_{Fast} is reduced while Q_{Med} and Q_{Slow} increase, following the exponential time course of channel opening (solid curves Fig. 6 E) (Horrigan and Aldrich, 1999, 2002). These kinetics are similar in the presence and absence of Mg^{2+} because 10 mM Mg^{2+} has little effect on activation kinetics (Shi and Cui, 2001; Zhang et al., 2001). However the relative amplitudes of Q_{Med} and Q_{Slow} are reversed by Mg^{2+}. The change in relative amplitude of Q_{Med} and Q_{Slow} by Mg^{2+} is qualitatively similar to the effect of recording I_{gOFF} at a more positive voltage in 0 Mg^{2+} (Horrigan and Aldrich, 1999), supporting that Mg^{2+} shifts Q_o to more negative voltages. In the absence of Mg^{2+}, Q_{Med} is greater than Q_{Slow} because voltage sensors can completely deactivate at −80 before channels close (Fig. 6 D, 0 Mg^{2+} light blue arrow). That is, the Q_o-V relation in 0 Mg^{2+} indicates that voltage sensors equilibrate to the resting state at −80 mV (Fig. 5 E). By contrast, in 10 Mg^{2+} more than 25% of voltage sensors should remain activated at −80 mV when channels are open (10 Mg^{2+} Q_o-V, Fig. 5 E). Consequently, channels can close from open states other than O_0 (e.g., O_2 in Fig. 6 D, 10 Mg^{2+}), and voltage sensor deactivation becomes rate limited by closing (Fig. 6 D, 10 Mg^{2+} pink arrow) such that the ratio of Q_{Slow} to Q_{Med} is increased.

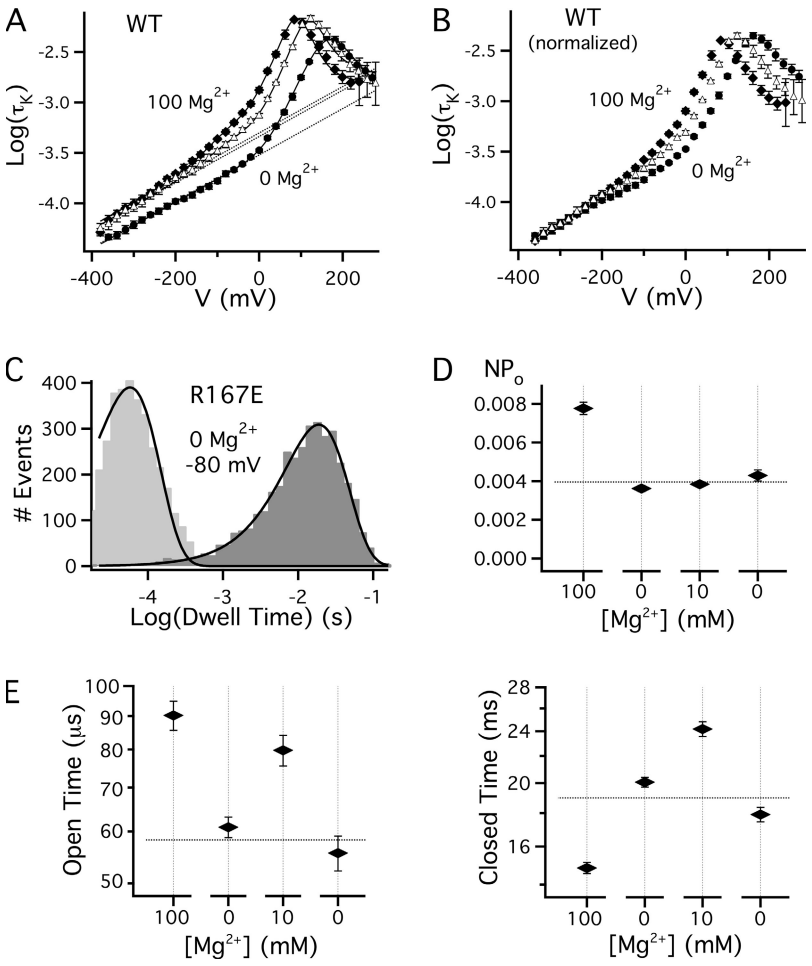

Figure 7. Effects of Mg^{2+} on I_K kinetics. (A) Mean log(τ_K)-V relations in 0 (●), 10 (△), and 100 (◆) mM Mg^{2+}. Dotted lines are fits to the limiting slope of τ_K between −380 and −240 mV with an exponential function with partial charge −0.135*e*. Solid curves are fits to Scheme 1* (Fig. 6 D) using parameters in Table III. (B) τ_K-V relations from A were normalized to the 0 Mg^{2+} relation based on the exponential fits. (C) Open and closed dwell-time histograms for R167E at −80 mV in 0 Mg^{2+} from a patch containing ∼10,000 channels. Dwell time histograms were log-binned and are fit by single exponential functions, consistent with a two-state closed–open transition when voltage sensors are in the resting state. (D) NP_O at −80 mV measured from steady-state recordings of 20-30 s total duration in the same patch as C as [Mg^{2+}] was changed in sequence from 100 mM to 0, 10 mM, and back to 0 Mg^{2+}. The data were acquired in 5-s traces and error bars represent the standard error of measurements from individual traces. (E) Mean open and closed times corresponding to D. Dotted lines in D and E indicate the mean value in 0 Mg^{2+}.

Effects of Mg^{2+} on I_K Kinetics

The ability to slow channel closing is a characteristic of Mg^{2+} action at the RCK1 site that is evident by comparing I_K tail currents at −80 mV in 0 and 10 mM Mg^{2+} (Fig. 2 A). Time constants of I_K relaxation (τ_K) plotted versus voltage in Fig. 7 A for 0, 10, and 100 mM Mg^{2+} indicate that 10 mM Mg^{2+} slows I_K deactivation approximately twofold over a wide voltage range (−380 to +100 mV) with little impact on activation kinetics at very positive voltages (+160 to +280 mV). By contrast, increasing Mg^{2+} from 10 to 100 mM to occupy very low affinity sites speeds activation with no additional effect on deactivation at extreme negative voltages (Fig. 7 A) (Zhang et al., 2001; Hu et al., 2006).

That 10 and 100 mM Mg^{2+} have distinct effects on τ_K is not surprising given their action at different binding sites. However, the effects of Mg^{2+} on deactivation kinetics are remarkable in comparison to the effects on steady-state activation. Macroscopic I_K kinetics are rate limited by the C-O transition (Horrigan and Aldrich, 1999) and at sufficiently negative voltages by the O_0 to C_0 rate constant (Fig. 6 D, top). Thus, the ability of 10 Mg^{2+} to slow deactivation at extreme negative voltages is surprising given that 10 mM Mg^{2+} has no detectable effect on the equilibrium constant for the C_0-O_0 transition (L_0). Similarly, the failure of 100 Mg^{2+} to slow deactivation relative to 10 Mg^{2+} is notable because 100 Mg^{2+} increases L_0.

Although previous studies have shown that Mg^{2+} slows deactivation at voltages as low as –200 mV, measurements at more negative voltage were required to confirm that the O_0 to C_0 transition rate is altered. Because Mg^{2+} shifts the Q_o-V relation, channels can close by pathways involving different C-O transitions in the presence and absence of Mg^{2+} (e.g., Fig. 6 D). This difference contributes to the slowing of tail currents in Mg^{2+} at −80 mV. However at sufficiently negative voltages, τ_K should be limited only by the O_0 to C_0 transition whether or not Mg^{2+} is present. Consistent with this prediction, at voltages less than −240 mV the difference in τ_K between 10 and 100 mM Mg^{2+} is almost eliminated and τ_K achieves a limiting voltage dependence that is identical in the presence or absence of Mg^{2+} (Fig. 7 A, dotted lines). Normalized τ_K-V relations (Fig. 7 B) illustrate that a major effect of Mg^{2+} is to shift the τ_K-V relation along the voltage axis, consistent with effects on Q_o. However, the ability of 10 mM Mg^{2+} to increase τ_K 1.53-fold at $V < -240$ mV confirms that the O_0 to C_0 rate is also reduced.

TABLE III

Scheme 1 Parameters*

	Rate Constants (s^{-1})					
$[Mg^{2+}]$(mM)	γ_0	δ_0	δ_1	δ_2	δ_3	δ_4
0	3330	.0035	.091	1.9	22.6	101
10	2140	.0023	.061	4.9	163	71
100	1980	.0051	.098	8.6	265	94

Rate constants for the C_i-O_i transitions in Scheme 1* (Fig. 6 D) determined from fits to WT τ_K-V relations in 0-100 mM Mg^{2+} (Fig. 7 A), using equilibrium parameters from Table I (WT, WT_B). Since voltage sensor activation equilibrates rapidly, τ_K was fit by $\tau_K = \left[\sum\left(\delta_i\ pC_i + \gamma_i\ pO_i\right)\right]^{-1}$, where i represents the number of activated voltage sensors, δ_i and γ_i are forward and backward rate constants for the C_i-O_i transitions and pC_i, pO_i are conditional occupancies of the open and closed states ($pC_i = p(C_i|C)$, $pO_i = p(O_i|O)$) (Horrigan et al., 1999). Forward rates (δ_i) were varied while backward rates were $\gamma_i = \delta_i/L_0D^i$ and partial charges associated with these rate constants were $z_\delta = 0.165e$ and $z_\gamma = -0.135e$ (Horrigan and Aldrich, 2002).

That the kinetics of the C_0-O_0 transition are affected by 10 mM Mg^{2+} without altering the equilibrium constant suggests that both the forward and reverse rate constants for this transition must be slowed. To test this hypothesis we analyzed unitary current kinetics from a macropatch containing R167E channels at −80 mV where voltage sensors should be in the resting state. Although the patch contained an estimated 10,000 channels, >99% of openings were to the single channel level because P_O at this voltage is low (4×10^{-7} in 0 Mg^{2+}, Fig. 5 D). Both open and closed dwell times histograms were reasonably fit by single exponential components as illustrated for 0 Mg^{2+} in Fig. 7 C, consistent with a two-state C_0-O_0 transition. Changes in NP_O (Fig. 7 D) and mean open and closed times (Fig. 7 E) are plotted as $[Mg^{2+}]$ was changed in sequence from 100 mM to 0, 10, and back to 0 Mg^{2+}. The results show that the change from 0 to 10 mM Mg^{2+} increases both open and closed times, consistent with a similar slowing of both forward and backward rates of channel opening that leaves NP_O unchanged. Open times were brief but comparable to the ∼100-μs time constant of macroscopic I_K measured for this patch at −80 mV in 0 Mg^{2+}. The frequency of channel openings was reversibly reduced by 10 mM Mg^{2+} as expected from the effect on mean closed times. In a patch with N independent channels and brief openings the mean closed time should equal N/(opening rate), implying that the mean closed time of individual channels was ∼3–4 min. Increasing Mg^{2+} from 10 to 100 mM only slightly increased open times but markedly decreased closed times, consistent with the ability of 100 Mg^{2+} to increase NP_O without changing τ_K relative to 10 mM Mg^{2+} at negative voltages. These conclusions about the C_0-O_0 transition from single-channel analysis are consistent with effects of Mg^{2+} on rate constants in Scheme 1* (δ_0, γ_0) derived by fitting the macroscopic data (Fig. 7 A, solid curves, Table III parameters).

The effect of Mg^{2+} on the kinetics of the C_0-O_0 transition is important in providing mechanistic information that is not evident from the steady-state data. In particular, the ability of 10 mM Mg^{2+} to slow opening and closing rates demonstrates that Mg^{2+} remains bound to the RCK1 site and can influence channel gating when voltage sensors are in the resting state even though P_O is insensitive to Mg^{2+} under these conditions.

DISCUSSION

Our results show that intracellular Mg^{2+} activates Slo1 BK channels through a fundamentally different mechanism from Ca^{2+}. While micromolar $[Ca^{2+}]_i$ promotes channel opening independent of voltage sensor activation, millimolar $[Mg^{2+}]_i$ acting at a putative binding site in the cytosolic RCK1 domain has effects on opening and voltage sensor activation that are highly interdependent. Mg^{2+} promotes opening only when voltage sensors are activated and facilitates voltage sensor activation mainly when channels are open. Because Mg^{2+} action depends on the conformation of both voltage sensor and gate, the primary effect on gating is to enhance voltage sensor/gate coupling such that open-activated states are stabilized. A two-site allosteric model that incorporates this mechanism reproduces the major effects of Mg^{2+} on steady-state activation. As discussed below, these results support that multiple pathways of communication exist between the cytosolic and transmembrane domains of BK channels. Our data also constrain the possible physical mechanisms that underlie Mg^{2+}-dependent activation and voltage sensor/gate coupling, and suggest that the physiological impact of Mg^{2+} could differ qualitatively from that of Ca^{2+}.

Communication between Cytosolic and Transmembrane Domains

Ca^{2+} has no effect on voltage sensor/gate coupling (Horrigan and Aldrich, 2002) and is thought to promote channel opening by pulling on the RCK1–S6 linker (Niu et al., 2004). Therefore, the ability of Mg^{2+} to enhance coupling suggests that the cytosolic domain can communicate with the transmembrane domain through pathways other than the RCK1–S6 linker, presumably involving direct or indirect interactions with the voltage sensor (e.g., Fig. 1 D). A similar conclusion was drawn from the effects of intracellular heme (Horrigan et al., 2005).

However, the action of Mg^{2+} is remarkable in its simplicity and specificity relative to heme. While heme weakens voltage sensor/gate coupling, it also reduces the efficacy of Ca^{2+} and increases P_O at extreme negative voltages (i.e., increases L_0). These diverse effects on gating, together with a slow onset of action (minutes), suggest that heme binding may perturb the normal conformation of the cytosolic domain such that tension in the RCK1–S6 linker is increased while multiple allosteric interactions are also disrupted (Horrigan et al., 2005). In contrast, 10 mM Mg^{2+} does not alter Ca^{2+} sensitivity (Shi and Cui, 2001; Zhang et al., 2001) and acts rapidly (<1 s) at the RCK1 binding site to enhance voltage sensor/gate coupling without affecting the intrinsic stability of the gate (L_0). The effect of Mg^{2+} is complimentary to that of Ca^{2+}, which increases L_0 with no effect on coupling (Horrigan and Aldrich, 2002). Thus Mg^{2+} and Ca^{2+} appear to independently regulate two different pathways of communication, consistent with their additive effects on channel activation. Unlike heme, the effects of Mg^{2+} do not suggest a widespread structural perturbation, and can be understood in terms of stabilizing particular channel states.

The Energetic Effects of Mg^{2+}

Mg^{2+} at the RCK1 site acts primarily to stabilize the open-activated (OA) state relative to the other three states (CR, CA, and OR) defined by the voltage sensor and gate conformation in each subunit (Fig. 5 H; Table II). We reached this conclusion by measuring independently each of the equilibrium constants between these states, in effect determining their relative free energies in the presence and absence of Mg^{2+}, as specified by three independent parameters (L_0, J_0, and D). The CR-OR equilibrium constant (L_0) is not altered. The CR-CA equilibrium constant (J_0) is only increased slightly. However, the CA-OA and OR-OA equilibria are substantially altered, consistent with an approximate twofold increase in the voltage sensor/gate coupling factor D. By comparing the effects of Mg^{2+} on WT and mutant (E374A/E399N) channels, we showed that all changes in voltage sensor/gate coupling and a fraction of the changes in J_0 can be attributed to the RCK1 site. Modeling the effects of Mg^{2+} in terms of a two-site allosteric scheme (Table II) suggests that saturating the RKC1 site (site 1) stabilizes the OA state relative to CR by $\Delta\Delta G_{CR}^{OA} = kTln(E_1F_1) = 0.60$ kcal mol^{-1}, while stabilizing the CA state by $\Delta\Delta G_{CR}^{CA} = kTln(E_1) = 0.18$ kcal mol^{-1}. Thus the energetic effect of Mg^{2+} is weak compared with that of Ca^{2+} binding or voltage sensor activation (1.25 or 1.91 kcal mol^{-1} per subunit) (Horrigan and Aldrich, 2002).

Parallel Pathways of Voltage Sensor/Gate Coupling

While the interactions that couple voltage sensor activation to channel opening are well defined energetically, they could reflect many different physical mechanisms. The coupling represents a differential effect of voltage sensor conformation on the free energy of closed and open states. Therefore voltage sensor and gate must interact in a state-dependent manner that depends on the conformation of both domains. Such interactions could represent a stabilizing interaction (e.g., bond formation) between voltage sensor and gate that occurs only in the OA state, or destabilizing interactions (e.g., steric or repulsive) that occur in every state but OA. Alternatively, sensor and gate could be coupled in all states by a spring-like connection whose tension varies with both voltage sensor activation and channel opening.

Any of the above or similar mechanisms, alone or in combination, could contribute to the allosteric coupling factor D. Thus the ability of Mg^{2+} to increase D does not require that interactions that normally mediate coupling in the absence of Mg^{2+} are enhanced. Indeed, two lines of evidence suggest that the effect of Mg^{2+} represents a parallel pathway of coupling, independent of that in the transmembrane domain (Fig. 8 A). First, Mg^{2+} in the RCK1 binding site appears to interact with a part of the voltage sensor that is not important for voltage sensor/gate coupling in the absence of Mg^{2+}. Interactions of the S4–S5 linker near S5 with S6 are proposed to mediate coupling in Kv channels (Lu et al., 2002; Long et al., 2005b). Although mutations in the S4–S5 linker of Slo1 influence Mg^{2+} sensitivity (Hu et al., 2003), they are at sites near S4 (E219, Q222) that are unlikely to interact directly with S6. In addition, mutations of R213 in S4 virtually abolish Mg^{2+} sensitivity (Hu et al., 2003; Yang et al., 2007), but have no effect on voltage sensor/gate coupling in 0 Mg^{2+} (Ma et al., 2006). Second, interactions between the voltage sensor and Mg^{2+}-binding site should be sufficient to influence voltage sensor/gate coupling, because the binding site is in a cytosolic domain attached to S6 and therefore is connected to the gate.

Physical Mechanism of Mg^{2+} Action

Since Mg^{2+} stabilizes primarily the OA state, thermodynamics require that Mg^{2+} affinity is greatest in the OA state, as in Scheme 3. However, the conclusion that Mg^{2+} binding is favored in a particular state does not fully describe how and when Mg^{2+} interacts with its binding site and the voltage sensor. If we suppose that the interactions of Mg^{2+} with its binding site are purely stabilizing, then interactions must exist in the OA state that are stronger or more numerous than in other conformations. Such a situation could arise if both the cytosolic and voltage sensor domains contribute to the Mg^{2+} binding site, but are favorably aligned with each other only when the voltage sensor is activated and the channel is open. However, this hypothesis appears too simple given recent evidence that a destabilizing electrostatic interaction exists between Mg^{2+} and the voltage sensor (Yang et al., 2007); and physical models that take this into account are necessarily more complex, as discussed below.

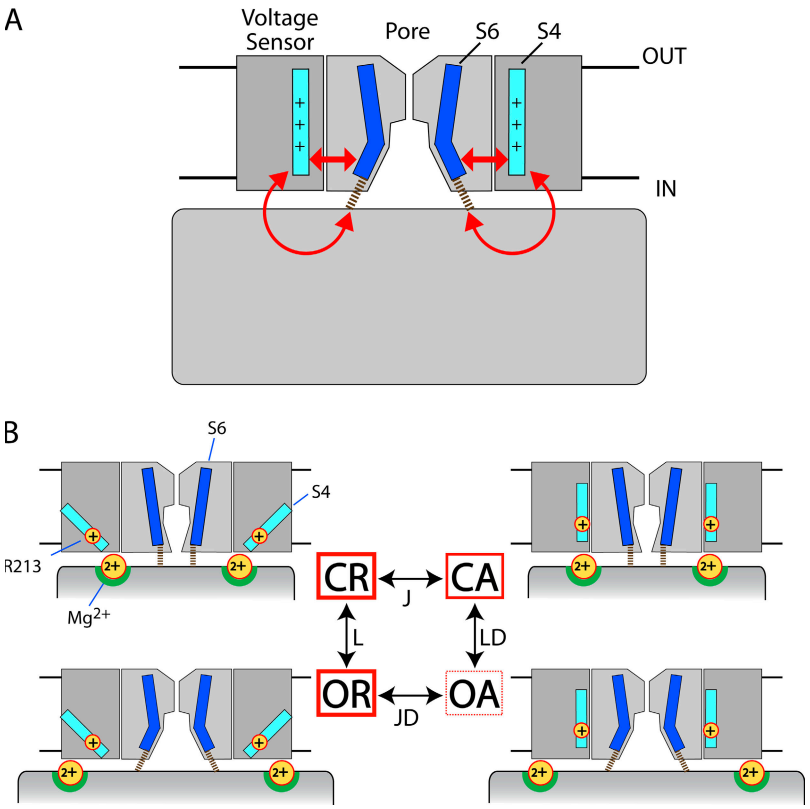

Figure 8. Voltage sensor/gate coupling and the mechanism of Mg^{2+} action. (A) Multiple pathways of voltage sensor/gate coupling may exist in BK channels. Because the cytosolic domain is connected to the gate via the RCK1–S6 linker (dashed line), interactions between cytosolic and voltage sensor domains could provide a coupling pathway (curved arrow) that is independent of that within the transmembrane domain (straight arrow). (B) A speculative model of Mg^{2+}-dependent activation, based on an electrostatic mechanism of interaction between Mg^{2+} in the putative RCK1 binding site and R213 in S4 (Yang et al., 2007). The BK channel is shown in the four states defined in each subunit by the movement of the voltage sensor from resting (R) to activated (A) and by the closed (C) to open (O) conformational change. Channel opening is accompanied by an expansion of the cytosolic domain that alters the position of Mg^{2+} (in its binding site) relative to the transmembrane domain. The Mg^{2+} binding site (green semicircle) in the RCK1 domain includes coordinating residues E374 and E399 and nearby Q397 (Yang et al., 2006). Voltage sensor activation moves R213 relative to the cytosolic domain. In this way the distance and therefore electrostatic repulsion between Mg^{2+} and R213 (indicated qualitatively by the thickness of red boxes surrounding each state) depends on the conformation of both voltage sensor and gate, such that voltage sensor/gate coupling is enhanced. To account for the observed effects of Mg^{2+} on both opening and voltage sensor activation requires that the OA state be stabilized (see text). This is accomplished in the model by maintaining a similar distance between Mg^{2+} and R213 in all states except OA, such that all states are destabilized relative to OA. To account for a small effect of Mg^{2+} on voltage sensor activation when channels are closed we also assume interaction in the CA state is slightly weaker than the CR state, owing to a small outward movement of R213 upon voltage sensor activation, consistent with the small contribution of R213 to gating charge (Ma et al., 2006).

The effects on Mg^{2+} sensitivity and gating of charge-altering mutations in the voltage sensor and RCK1 domain strongly suggest that Mg^{2+} activates the channel through a long-range electrostatic interaction with R213 in S4 (Yang et al., 2007). Addition of positive charge at position 397 near the RCK1 site (Yang et al., 2006), by either mutation (Q397K, Q397R) or chemical modification, mimics the major effects of Mg^{2+} on channel gating; whereas negative charge at this position (Q397E, Q397D) inhibits activation. Conversely a positive charge at position 213 appears necessary for sensing either Mg^{2+} or charge at position 397. Finally, the effects on gating of Mg^{2+} or Q397K but not Ca^{2+} are strongly inhibited in high ionic strength solutions (1 M KCl), consistent with a long-range electrostatic interaction between Mg^{2+} and the voltage sensor. Based on these results, Yang et al. propose that Mg^{2+} bound to the RCK1 domain alters the local electric field sensed by R213 in S4 and thereby promotes voltage sensor activation. That is, electrostatic repulsion between Mg^{2+} and R213 destabilizes the resting conformation of the voltage sensor. This interaction is presumably state dependent since voltage sensor activation is enhanced by Mg^{2+} primarily when the channel is open.

The observations of Yang et al. (2007) together with our functional analysis place important constraints on the physical nature and state dependence of the interactions underlying Mg^{2+}-dependent activation. Most importantly, the ability of R213 mutants to virtually eliminate Mg^{2+} sensitivity suggests that the electrostatic interaction between R213 and Mg^{2+} accounts for the major effects of Mg^{2+} on gating, and therefore must act on balance to stabilize the OA state. This conclusion has two key implications. First, the coordination of Mg^{2+} at its binding site cannot be strongly state dependent. If it were, then the channel's Mg^{2+} affinity should change in a state-dependent manner even in the absence of electrostatic interaction with S4; and gating should therefore remain Mg^{2+} sensitive when R213 is mutated. Although subtle effects of this sort cannot be ruled out, R213 mutations largely eliminate the G_K-V shift and slowing of I_K deactivation by Mg^{2+} (Hu et al., 2003; Yang et al., 2007). Thus it appears unlikely that conformational changes in the binding site associated with channel opening favor Mg^{2+} binding and contribute to Mg^{2+}-dependent activation. This conclusion is supported by the observation that a permanent positive charge at position 397 mimics the effects of Mg^{2+} (Yang et al., 2007). Second, if Mg^{2+}

stabilizes the OA state via a destabilizing electrostatic interaction, then the interaction must be weakest in the OA state and of similar strength in all other states (CR, CA, OR). That is, Mg^{2+} must destabilize all states relative to OA.

That Mg^{2+} interacts with the voltage sensor in multiple states including closed states may seem counterintuitive since Mg^{2+} has little effect on voltage sensor activation when channels are closed. Indeed, interaction in a single state, open resting (OR), would be sufficient to account for the ability of Mg^{2+} to promote voltage sensor activation when channels are open, by destabilizing OR relative to OA. However, this simple model cannot account for the effects of Mg^{2+} on channel opening. If the OR state is destabilized without also destabilizing the CR state then channel opening should be inhibited when voltage sensors are in the resting state, inconsistent with our finding that L_0 is unaffected by 10 mM Mg^{2+}. Conversely, a lack of interaction between Mg^{2+} and the activated voltage sensor would be inconsistent with the ability of Mg^{2+} to facilitate opening of R210C channels when voltage sensors are constitutively activated. Thus accounting for effects of Mg^{2+} on both channel opening and voltage sensor activation requires that multiple states are destabilized.

The conformational changes that allow Mg^{2+} to interact with the voltage sensor in a state-dependent manner are not known in detail. However, a speculative model consistent with our results is illustrated in Fig. 8 B. The model assumes that Mg^{2+} and the voltage sensor interact electrostatically in all states but that the interaction is weakest in the OA state (as indicated by red boxes). Consequently, the OA state has the highest affinity for Mg^{2+} because the voltage sensor repels Mg^{2+} the least. For illustration purposes, interaction strength is assumed to vary with changes in the distance between Mg^{2+} and the charged R213 sidechain, although changes in local dielectric environment could also be involved. Fig. 8 B shows how the distance between Mg^{2+} and R213 could remain relatively constant in all states other than OA if the position of the Mg^{2+}-binding site moves with channel opening and R213 moves with voltage sensor activation.

The insensitivity of P_O to Mg^{2+} at extreme negative voltages is accounted for in Fig. 8 B by assuming the Mg^{2+} binding site in the closed and open conformation occupies two different locations that are equidistant from R213 in the resting state. In this way the CR and OR states are equally destabilized. Interestingly, this mechanism is also consistent with our finding that Mg^{2+} slows both opening and closing rates when voltage sensors are in the resting state. This kinetic effect implies that Mg^{2+} destabilizes a transition state between CR and OR. In Fig. 8 B, movement of the Mg^{2+} binding site between closed and open positions would allow Mg^{2+} to approach R213 more closely in a transition state than in either the CR or OR states, thereby destabilizing the transition state.

Although the details of Fig. 8 B are speculative, they are consistent with known features of BK and related channels. The location and movement of the Mg^{2+}-binding site relative to R213 is based on the crystal structures of MthK and Kv1.2. Residues in MthK (E138, N158), corresponding to E374 and E399 in the putative Mg^{2+} binding site of Slo1, are on the surface of the gating ring facing the membrane at a distance from the central axis of the channel (~31 Å) that roughly matches the radial position of the S4 segment in Kv1.2 (Yang et al., 2007). The Mg^{2+}-binding site is shown to move away from the central axis upon channel opening, consistent with an expansion of the cytosolic domain as in MthK (Jiang et al., 1999; Ye et al., 2006). Voltage sensor activation is depicted as a tilt and outward translation of S4 that is qualitatively consistent with recent models of Kv channel activation (Ruta et al., 2005; Campos et al., 2007; Pathak et al., 2007). We have assumed that movement of R213 perpendicular to the membrane is small such that interaction with Mg^{2+} in the CA state is not disrupted. This assumption is consistent with the fact that Slo1 is weakly voltage dependent and neutralization of R213 reduces the gating charge associated with voltage sensor activation (z_J) by only 0.3 *e* (Ma et al., 2006).

One possibility that was not incorporated into Fig. 8 B is that the position of R213 in the transmembrane domain may change with channel opening. Previous results suggest that R213 moves relative to the membrane electric field during opening because mutations at this position reduce the charge associated with opening (z_L) (Ma et al., 2006). If the position of R213 depends on the conformation of both voltage sensor and gate then the requirement that the Mg^{2+}-binding site move during channel opening may be reduced. Therefore, Fig. 8 B does not represent a unique solution, but it does illustrate the constraints that must be satisfied to account for the experimental data in terms of electrostatic interactions.

Very Low Affinity Mg^{2+} Binding Sites

Divalent cation binding sites with lower affinity for Mg^{2+} than the RCK1 site are proposed to exist in BK channels because G_K-V shifts produced by increasing [Mg^{2+}] or [Ca^{2+}] from 10 to 100 mM appear too large to represent surface charge screening (Zhang et al., 2001) and are nearly independent of mutations that eliminate responses to lower concentrations of Mg^{2+} or Ca^{2+} (Hu et al., 2006). The location, number, and physiological significance of these very low affinity sites are unknown. However, our results provide new information about their mechanism of action.

We find that 100 mM Mg^{2+}, unlike 10 mM Mg^{2+}, increases L_0 and causes a shift in V_{hC} that is only partially

eliminated by mutating the RCK1 site. These effects can be reproduced by an allosteric mechanism (Scheme 2) similar to that used to describe effects of micromolar Ca^{2+}. However, very low affinity sites and Ca^{2+} sites differ greatly in the relative magnitude of their effects on the gate and voltage sensor represented by allosteric factors C and E, respectively. The G_K-V shift by Ca^{2+} is dominated by a C-factor of 8, which results in a 4,000-fold increase in P_O at −120 mV (Horrigan and Aldrich, 2002). By contrast the very low affinity site (C = 1.6) increases P_O (−120 mV) approximately threefold in 100 mM Mg^{2+}, sufficient to account for only one third of the G-V shift from 10 to 100 mM Mg^{2+}. The majority of the G-V shift in high [Mg^{2+}] reflects a change in V_{hC}, which was attributed to an E-factor of 2.3.

The ability of 100 mM Mg^{2+} to increase L_0 supports that the effects of high [Mg^{2+}] reflect mechanisms other than surface charge screening. However, the possibility remains that surface charge screening contributes to V_{hC}. Hu et al. (2006) estimated, based on surface potential calculations, that such a mechanism could shift V_{hC} by ∼−9 mV from 10 to 100 mM Mg^{2+}, which is roughly half of the observed ΔV_{hC} (−19 mV) for the WT over this concentration range. Therefore, although we were able to model the effects of Mg^{2+} in terms of a single very low affinity site per subunit this is likely an oversimplification. The E-factor in our model could represent a combination of allosteric and surface charge effects. In addition, we observed a decrease in G_K-V slope from 10 to 100 Mg^{2+} that was not accounted for by our model.

Relation to Previous Studies and Physiological Implications

Since Mg^{2+} and Ca^{2+} act through distinct mechanisms, it seems surprising that previous studies were able to model effects of Mg^{2+} on the G_K-V relation, in the presence and absence of Ca^{2+}, by assuming Mg^{2+} and Ca^{2+} act through the same mechanism (Shi and Cui, 2001; Zhang et al., 2001; Hu et al., 2006). This comparison raises several questions addressed below. First, can our model account for previous observations that the G_K-V shift by Mg^{2+} is similar in the presence or absence or presence of Ca^{2+}? Second, were conclusions of previous studies affected by the use of a Ca^{2+}-like model of Mg^{2+} action? Third, is the difference in mechanism of Mg^{2+} and Ca^{2+} action physiologically significant?

Although our experiments were performed in 0 Ca^{2+}, we simulated the effect of saturating Ca^{2+} on our two-site model of Mg^{2+}-dependent activation (Eq. 2) by increasing the values of L_0 (4096-fold) and J_0 (2.4-fold) as predicted from previous work on Ca^{2+}-dependent activation (Horrigan and Aldrich, 2002). This simulation predicts that an increase in [Mg^{2+}] from 0 to 100 mM will shift $V_{0.5}$ by −105 mV and −78 mV in 0 and saturating Ca^{2+}, respectively, similar to the experimental results measured from Zhang et al. (2001) in 0 Ca^{2+} (−104 mV) and 300 μM Ca^{2+} (−72 mV). Thus our model appears to reproduce the combined effects of Mg^{2+} and Ca^{2+} on steady-state activation.

Conclusions about the Mg^{2+} affinity of the RCK1 site should be relatively unaffected by the incorrect assumption that Mg^{2+} acts through a Ca^{2+}-like mechanism. Previous studies assumed that Mg^{2+} increases the C-O equilibrium constant L_0 by binding with higher affinity to the open rather than closed conformation (Shi and Cui, 2001; Zhang et al., 2001; Hu et al., 2006). Similarly, our model of the RCK1 site (Scheme 3) assumes the Mg^{2+} affinity of the open-activated (OA) state is greater than any other state. That is, Mg^{2+} does bind better to the open conformation than the closed, so long as the probability that an open channel is in the OA state is high. This probability is indicated by the Q_o-V relation, which is saturated at voltages where the G-V is usually measured (Fig. 5, compare A and E). Therefore, Scheme 3 affects the G-V relation similar to models that assume Mg^{2+} binds equally well to all open states. Consistent with this similarity a previous study using a two-site Ca^{2+}-like model of Mg^{2+} action estimated K_D values for the RCK1 site of 5.46 mM (closed) and 2.25 mM (open) (Hu et al., 2006), comparable to our estimates based on Eq. 2 (K_D(CR) = 5 mM, K_D(CA) = 3.7 mM, K_D(OA) = 1.85 mM).

The physiological impact of Mg^{2+}-dependent BK channel activation has yet to be defined. However, our results raise the possibility that Mg^{2+} could have a differential impact on BK-dependent processes such as action potential shaping in neurons and the control of vascular smooth muscle tone. Both these processes require an increase in $[Ca^{2+}]_i$ to open BK channels that are poorly activated by resting $[Ca^{2+}]_i$ at physiological voltages. During an action potential, Ca^{2+} influx through voltage-dependent Ca^{2+} channels together with membrane depolarization activates BK channels to regulate spike duration and the fast afterhyperpolarization (Faber and Sah, 2003). By contrast, BK channels in vascular smooth muscle can contribute to resting membrane potential and myogenic tone by activating at hyperpolarized voltages, near −40 mV, in response to local Ca^{2+} release from internal stores (Ca^{2+} sparks) (Brayden and Nelson, 1992; Wellman and Nelson, 2003). Since physiological concentrations of free Mg^{2+} (0.4–3 mM) (Gupta et al., 1984; Romani and Scarpa, 1992) are sufficient to shift the G_K-V relation (Hu et al., 2006) and the effects of Mg^{2+} and Ca^{2+} on $V_{0.5}$ are approximately additive, one might suppose that Mg^{2+} simply increases P_o during any Ca^{2+} transient; enhancing apparent Ca^{2+} sensitivity. However, our results suggest this is not the case. The effect of Mg^{2+}, unlike Ca^{2+}, depends on voltage sensor activation and is greatly diminished at hyperpolarized potentials (Fig. 2 C). Therefore, Mg^{2+} might be expected to have a smaller impact on vascular smooth muscle tone than on action potential shaping. Of course

determining the magnitude of such differences and the overall contribution of Mg^{2+} to BK channel physiology must await further investigation.

We thank Drs. Jianmin Cui and Toshinori Hoshi for helpful comments and Kin Yu Wong for excellent technical assistance.

This work was supported by a grant from the National Institutes of Health (NS42901) to F.T. Horrigan. An abstract of this work was presented at the 49th Annual Meeting of the Biophysical Society (2005).

Olaf S. Andersen served as editor.

Submitted: 4 September 2007
Accepted: 29 November 2007

REFERENCES

Armstrong, C.M., and F. Bezanilla. 1974. Charge movement associated with the opening and closing of the activation gates of the Na channels. *J. Gen. Physiol.* 63:533–552.

Avdonin, V., X.D. Tang, and T. Hoshi. 2003. Stimulatory action of internal protons on Slo1 BK channels. *Biophys. J.* 84:2969–2980.

Brayden, J.E., and M.T. Nelson. 1992. Regulation of arterial tone by activation of calcium-dependent potassium channels. *Science.* 256:532–535.

Butler, A., S. Tsunoda, D.P. McCobb, A. Wei, and L. Salkoff. 1993. mSlo, a complex mouse gene encoding "maxi" calcium-activated potassium channels. *Science.* 261:221–224.

Campos, F.V., B. Chanda, B. Roux, and F. Bezanilla. 2007. Two atomic constraints unambiguously position the S4 segment relative to S1 and S2 segments in the closed state of Shaker K channel. *Proc. Natl. Acad. Sci. USA.* 104:7904–7909.

Cox, D.H., J. Cui, and R.W. Aldrich. 1997. Allosteric gating of a large conductance Ca-activated K^+ channel. *J. Gen. Physiol.* 110:257–281.

Cui, J., and R.W. Aldrich. 2000. Allosteric linkage between voltage and Ca^{2+}-dependent activation of BK-type mslo1 K^+ channels. *Biochemistry.* 39:15612–15619.

Cui, J., D.H. Cox, and R.W. Aldrich. 1997. Intrinsic voltage dependence and Ca^{2+} regulation of mslo large conductance Ca-activated K^+ channels. *J. Gen. Physiol.* 109:647–673.

Diaz, F., M. Wallner, E. Stefani, L. Toro, and R. Latorre. 1996. Interaction of internal Ba^{2+} with a cloned Ca^{2+}-dependent K^+ (hslo) channel from smooth muscle. *J. Gen. Physiol.* 107:399–407.

Faber, E.S., and P. Sah. 2003. Calcium-activated potassium channels: multiple contributions to neuronal function. *Neuroscientist.* 9:181–194.

Ferguson, W.B. 1991. Competitive Mg^{2+} block of a large-conductance, Ca^{2+}-activated K^+ channel in rat skeletal muscle. Ca^{2+}, Sr^{2+}, and Ni^{2+} also block. *J. Gen. Physiol.* 98:163–181.

Gupta, R.K., P. Gupta, and R.D. Moore. 1984. NMR studies of intracellular metal ions in intact cells and tissues. *Annu. Rev. Biophys. Bioeng.* 13:221–246.

Hamill, O.P., A. Marty, E. Neher, B. Sakmann, and F.J. Sigworth. 1981. Improved patch-clamp techniques for high-resolution current recording from cells and cell-free membrane patches. *Pflugers. Arch.* 391:85–100.

Herrington, J., and R.J. Bookman. 1995. Pulse Control. University of Miami Press, Miami, FL.

Horrigan, F.T., and R.W. Aldrich. 1999. Allosteric voltage gating of potassium channels II. Mslo channel gating charge movement in the absence of Ca^{2+}. *J. Gen. Physiol.* 114:305–336.

Horrigan, F.T., and R.W. Aldrich. 2002. Coupling between voltage sensor activation, Ca^{2+} binding and channel opening in large conductance (BK) potassium channels. *J. Gen. Physiol.* 120:267–305.

Horrigan, F.T., J. Cui, and R.W. Aldrich. 1999. Allosteric voltage gating of potassium channels I. Mslo ionic currents in the absence of Ca^{2+}. *J. Gen. Physiol.* 114:277–304.

Horrigan, F.T., S.H. Heinemann, and T. Hoshi. 2005. Heme regulates allosteric activation of the Slo1 BK channel. *J. Gen. Physiol.* 126:7–21.

Hu, L., J. Shi, Z. Ma, G. Krishnamoorthy, F. Sieling, G. Zhang, F.T. Horrigan, and J. Cui. 2003. Participation of the S4 voltage sensor in the Mg^{2+}-dependent activation of large conductance (BK) K^+ channels. *Proc. Natl. Acad. Sci. USA.* 100:10488–10493.

Hu, L., H. Yang, J. Shi, and J. Cui. 2006. Effects of multiple metal binding sites on calcium and magnesium-dependent activation of BK channels. *J. Gen. Physiol.* 127:35–49.

Jiang, Y., A. Lee, J. Chen, M. Cadene, B.T. Chait, and R. MacKinnon. 2002. Crystal structure and mechanism of a calcium-gated potassium channel. *Nature.* 417:515–522.

Jiang, Y., A. Pico, M. Cadene, B.T. Chait, and R. MacKinnon. 2001. Structure of the RCK domain from the *E. coli* K^+ channel and demonstration of its presence in the human BK channel. *Neuron.* 29:593–601.

Jiang, Z., M. Wallner, P. Meera, and L. Toro. 1999. Human and rodent MaxiK channel beta-subunit genes: cloning and characterization. *Genomics.* 55:57–67.

Long, S.B., E.B. Campbell, and R. Mackinnon. 2005a. Crystal structure of a mammalian voltage-dependent *Shaker* family K^+ channel. *Science.* 309:897–903.

Long, S.B., E.B. Campbell, and R. Mackinnon. 2005b. Voltage Sensor of Kv1.2: Structural Basis of Electromechanical Coupling. *Science.* 309:903–908.

Lu, Z., A.M. Klem, and Y. Ramu. 2002. Coupling between voltage sensors and activation gate in voltage-gated K^+ channels. *J. Gen. Physiol.* 120:663–676.

Ma, Z., X.J. Lou, and F.T. Horrigan. 2006. Role of charged residues in the S1-S4 voltage sensor of BK channels. *J. Gen. Physiol.* 127:309–328.

Neyton, J. 1996. A Ba^{2+} chelator suppresses long shut events in fully activated high-conductance Ca^{2+}-dependent K^+ channels. *Biophys. J.* 71:220–226.

Niu, X., X. Qian, and K.L. Magleby. 2004. Linker-gating ring complex as passive spring and Ca^{2+}-dependent machine for a voltage- and Ca^{2+}-activated potassium channel. *Neuron.* 42:745–756.

Pathak, M.M., V. Yarov-Yarovoy, G. Agarwal, B. Roux, P. Barth, S. Kohout, F. Tombola, and E.Y. Isacoff. 2007. Closing in on the resting state of the shaker K^+ channel. *Neuron.* 56:124–140.

Patton, C., S. Thompson, and D. Epel. 2004. Some precautions in using chelators to buffer metals in biological solutions. *Cell Calcium.* 35:427–431.

Romani, A., and A. Scarpa. 1992. Regulation of cell magnesium. *Arch. Biochem. Biophys.* 298:1–12.

Ruta, V., J. Chen, and R. MacKinnon. 2005. Calibrated measurement of gating-charge arginine displacement in the KvAP voltage-dependent K^+ channel. *Cell.* 123:463–475.

Shi, J., and J. Cui. 2001. Intracellular Mg^{2+} enhances the function of BK-type Ca^{2+}-activated K^+ channels. *J. Gen. Physiol.* 118:589–606.

Shi, J., G. Krishnamoorthy, Y. Yang, L. Hu, N. Chaturvedi, D. Harilal, J. Qin, and J. Cui. 2002. Mechanism of magnesium activation of calcium-activated potassium channels. *Nature.* 418:876–880.

Stefani, E., M. Ottolia, F. Noceti, R. Olcese, M. Wallner, R. Latorre, and L. Toro. 1997. Voltage-controlled gating in a large conductance Ca^{2+}-sensitive K^+ channel (hslo). *Proc. Natl. Acad. Sci. USA.* 94:5427–5431.

Tang, X.D., R. Xu, M.F. Reynolds, M.L. Garcia, S.H. Heinemann, and T. Hoshi. 2003. Haem can bind to and inhibit mammalian calcium-dependent Slo1 BK channels. *Nature.* 425:531–535.

Tsien, R., and T. Pozzan. 1989. Measurement of cytosolic free Ca^{2+} with quin2. *Methods Enzymol.* 172:230–262.

Vergara, C., R. Latorre, N.V. Marrion, and J.P. Adelman. 1998. Calcium-activated potassium channels. *Curr. Opin. Neurobiol.* 8:321–329.

Wellman, G.C., and M.T. Nelson. 2003. Signaling between SR and plasmalemma in smooth muscle: sparks and the activation of Ca^{2+}-sensitive ion channels. *Cell Calcium.* 34:211–229.

Xia, X.M., X. Zeng, and C.J. Lingle. 2002. Multiple regulatory sites in large-conductance calcium-activated potassium channels. *Nature.* 418:880–884.

Yang, H., L. Hu, J. Shi, and J. Cui. 2006. Tuning magnesium sensitivity of BK channels by mutations. *Biophys. J.* 91:2892–2900.

Yang, H., L. Hu, J. Shi, K. Delaloye, F.T. Horrigan, and J. Cui. 2007. Mg^{2+} mediates interaction between the voltage sensor and cytosolic domain to activate BK channels. *Proc. Natl. Acad. Sci. USA.* 104:18270–18275.

Ye, S., Y. Li, L. Chen, and Y. Jiang. 2006. Crystal structures of a ligand-free MthK gating ring: insights into the ligand gating mechanism of K^+ channels. *Cell.* 126:1161–1173.

Zhang, G., and F.T. Horrigan. 2005. Cysteine modification alters voltage- and Ca^{2+}-dependent gating of large conductance (BK) potassium channels. *J. Gen. Physiol.* 125:213–236.

Zhang, X., C.R. Solaro, and C.J. Lingle. 2001. Allosteric regulation of BK channel gating by Ca^{2+} and Mg^{2+} through a nonselective, low affinity divalent cation site. *J. Gen. Physiol.* 118:607–636.